Geomorphology 365 (2020) 107231

Contents lists available at ScienceDirect

Geomorphology

journal homepage: www.elsevier.com/locate/geomorph

Recent evolution of the Irrawaddy (Ayeyarwady) Delta and the impacts of anthropogenic activities: A review and remote sensing survey

Dan Chen [a], Xing Li [a,*], Yoshiki Saito [b,c], J. Paul Liu [d], Yuanqiang Duan [a], Shu'an Liu [a], Lianpeng Zhang [a]

[a] School of Geography, Geomatics and Planning, Jiangsu Normal University, Xuzhou 221116, China
[b] Estuary Research Center (EsReC), Shimane University, 1060, Nishikawatsu-Cho, Matsue 690-8504, Japan
[c] Geological Survey of Japan, AIST, Higashi 1-1-1, Tsukuba 305-8567, Japan
[d] Department of Marine, Earth & Atmospheric Sciences, North Carolina State University, Raleigh, NC 27695, USA

ARTICLE INFO

Article history:
Received 21 November 2019
Received in revised form 28 April 2020
Accepted 28 April 2020
Available online 20 May 2020

Keywords:
Delta evolution
Shoreline change
Fluvial geomorphology
Coastal geomorphology
Remote sensing
Human activities

ABSTRACT

Intensive studies have been conducted globally in the past decades to understand the evolution of several large deltas. However, despite being one of the largest tropical deltas, the Irrawaddy (Ayeyarwady) Delta has received relatively little attention from the research community. To reduce this knowledge gap, this study aims to provide a comprehensive assessment of the delta's evolution and identify its influencing factors using remote sensing images from 1974 to 2018, published literature and available datasets on the river, and human impacts in its drainage basin. Our results show that 1) Based on the topographic and geomorphological features, the funnel-shaped Irrawaddy Delta can be divided into two parts: the upper fluvial plain and the lower low-lying coastal plain; 2) The past 44-year shoreline changes show that overall accretion of the delta shoreline was at a rate of 10.4 m/year, and approximately 42% of the shoreline was subjected to erosion from 1974 to 2018. In the western coast, 60% of shoreline was under erosion with an average shoreline change rate of 0.1 m/year. In the east part, 81% of the shoreline was accreted with an average accretion rate of 24 m/year; 3) River channel geomorphological analysis indicates that three distributaries of the Irrawaddy, Bogale, and Toe have developed most active sandbars, which coincides with the amount of water they discharged (>50%). This implies that these three distributaries might be the currently most active channels in the delta; 4) The Irrawaddy mainstream in the Central Dry Zone (the original high sediment yield area) has become less braided and some tributaries have become increasingly straightened, which are highly likely related to reductions in sediment supply and peak flow induced by dam construction; 5) The large geomorphological adjustments at the two bifurcation points means that the diversions and fractions of water and sediment into the distributaries have likely already changed due to anthropogenic impacts.

Our comprehensive analysis suggests that increasing human activities have caused reductions in coarse sediment supply entering the coastal delta plain, further inducing the erosion of the major channels in the lowermost delta and the western delta coast, and the adjustments of fluvial and coastal geomorphology; meanwhile, deforestation and terrestrial mining have provided extra fine sediment, which is mainly transported by the monsoon-driven current to the eastern coast to in part maintain its rapid accretion. Given the situation of rapidly increasing population and climate change, the current natural equilibrium state of the delta setting will most likely be disturbed in the near future. Therefore, our work calls for more intensive monitoring- and modeling-based study in order to better understand the controlling factors influencing the delta evolution in the future.

Contents

* Corresponding author.
E-mail address: lixing@jsnu.edu.cn (X. Li).

https://doi.org/10.1016/j.geomorph.2020.107231
0169-555X/

1. Introduction

River deltas are among the most densely populated areas on Earth and contain highly valuable ecosystems. In recent decades, most deltas in the world have experienced severe degradation as a result of anthropogenic activities and climate change (Syvitski et al., 2009). The increasing global vulnerability of deltas has affected the livelihoods of millions of people living in these low-lying areas (Vörösmarty et al., 2009). Thus, many major world deltas, including the deltas of the Nile (Stanley and Warne, 1993), Yangtze (Yang et al., 2011), Yellow (Kong et al., 2015), Mississippi (Blum and Roberts, 2009), Mekong (Li et al., 2017, Liu et al., 2017), and Ganges-Brahmaputra-Meghna rivers (Dunn et al., 2018), have received considerable attention from scientists. However, in contrast to other deltas, a relative dearth of research exists on the Irrawaddy (also known as Ayeyarwady) Delta (Giosan et al., 2018; Grill et al., 2019).

The Irrawaddy is considered one of the major tropical river systems in the world (Syvitski et al., 2014). Its basin covers 60% of Myanmar's territory (Fig. 1) and is home to over 90% of the population of Myanmar, that is heavily dependent on the river and its resources for livelihood (Furuichi et al., 2009). The Irrawaddy Delta is one of the most populous areas in Myanmar; about 15 million of Myanmar's total population of 51 million currently reside on the delta's land area of 35,000 km^2 (Brakenridge et al., 2017). Of particular note is the Irrawaddy Basin, including the delta region, which hosts 89 Key

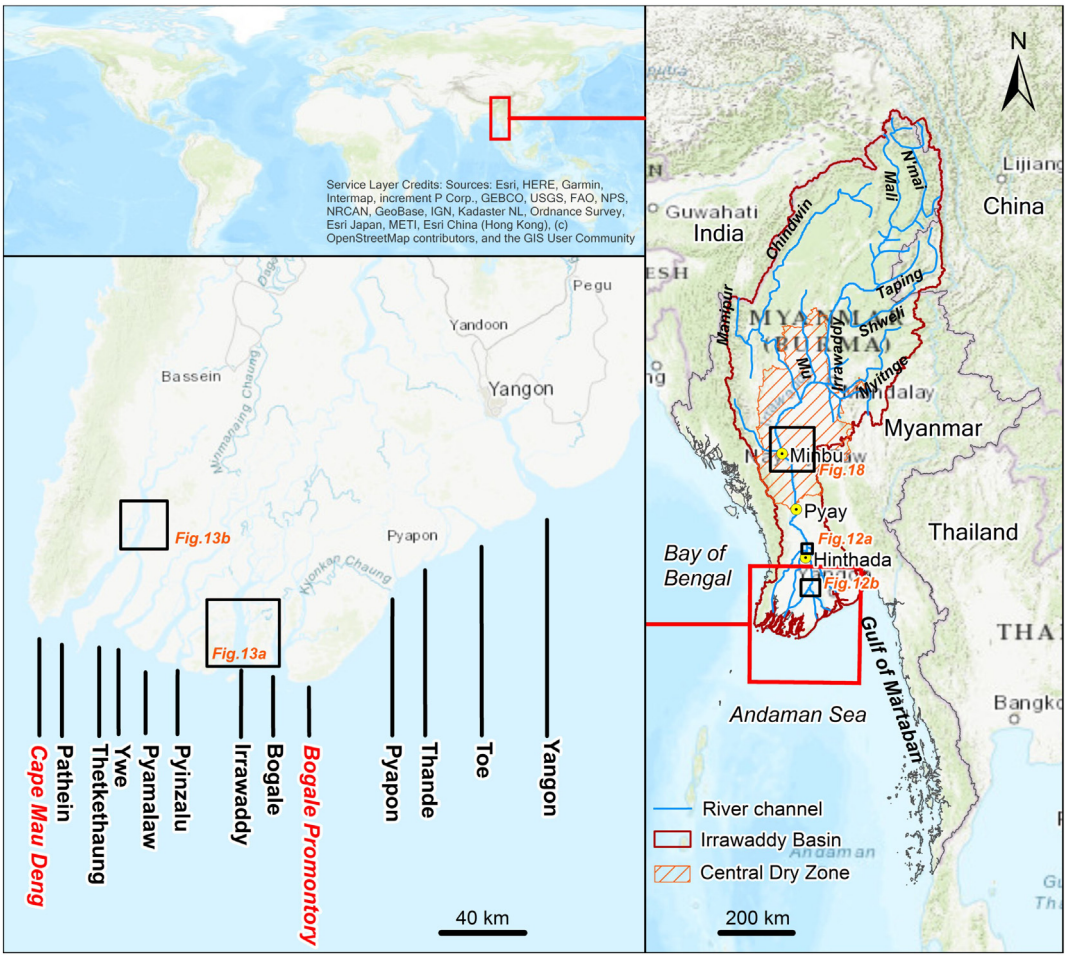

Fig. 1. Location of the Irrawaddy Delta and Basin. The black boxes indicate the spatial positions of other figures.

Biodiversity Area sites (KBAs) (HIC, 2017). Because of Myanmar's economic and political isolation, the Irrawaddy River and its delta have remained largely inaccessible for many years (Webb et al., 2014). However, the once pristine Irrawaddy has been considerably disturbed by increasing human activities, such as dam construction, agricultural development, deforestation, and terrestrial mining, throughout its basin in recent decades (Hennig, 2016). This has caused detectable changes in the hydrological regime of the Irrawaddy Basin (HIC, 2017). The Irrawaddy Delta is very low-lying and flat (Fig. 2), located at the sea level 200 km upstream from the Irrawaddy River mouths

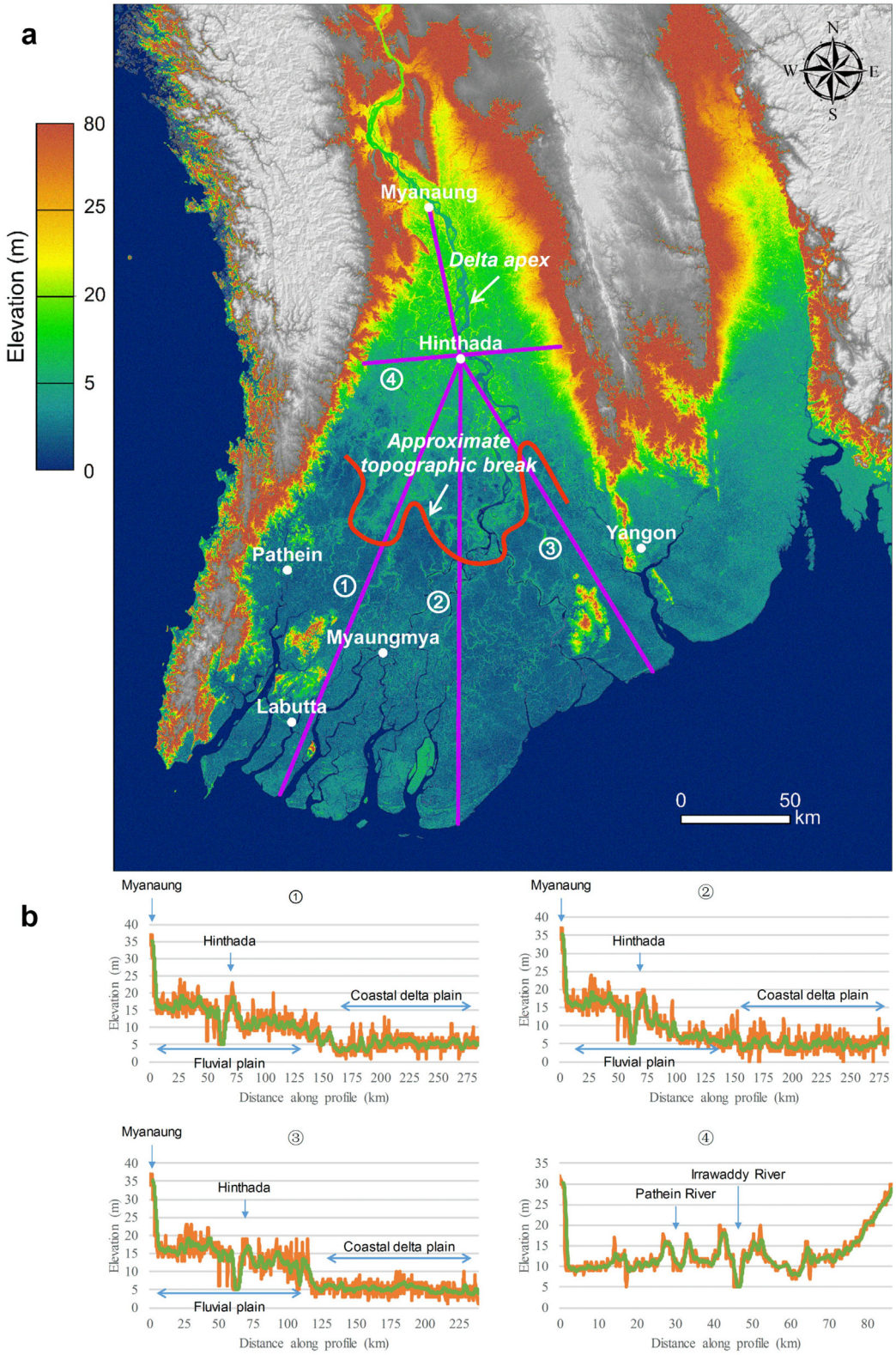

Fig. 2. (a) Digital elevation model created from the ASTER GDEM Version 2 data. The approximate topographic break shows the boundary between the fluvial plain and coastal delta plain. (b) The elevation profiles are based on the ASTER GDEM Version 2 data. These profiles can help identify physiographic features such as the fluvial plain and low-lying coastal delta plain; green lines represent running averages.

(Webster, 2008). This low elevation makes the delta particularly susceptible to flooding from tropical cyclones and storms. Cyclone Nargis in May 2008 inundated 40% of the delta's land area, killed over 130,000 people (Webster, 2008; Liu et al., 2020), and caused the delta's shoreline to retreat, on an average, by 47 m (Besset et al., 2017). The Irrawaddy Delta has been designated as "in peril" based on Syvitski et al. (2009). Increasing human disturbances, ecological degradation, and an anticipated sediment deficit will further increase the vulnerability of the delta to extreme events and coastal erosion.

The few studies related to the evolution of the Irrawaddy Delta can be classified within two time periods: pre-1990s and post-2005. The pre-1990s studies mainly involve hydrological surveys (Login, 1857; Gordon, 1879; Gordon, 1885; Halcrow, 1982; Brichieri-Columbi, 1983), earliest aerial surveys of the delta forests (Stamp, 1925), physical settings of the river (Stamp, 1940), and delineations of the delta's growth pattern (Stamp, 1940; Rodolfo, 1975). During the initial phase of the post-2005 period, researchers first reanalyzed a discharge and sediment load dataset from the 19th century (Robinson et al., 2007), provided a modern estimation (1969–1996) (Furuichi et al., 2009), and calculated the sediment contributions from tributaries (Garzanti et al., 2016). Several recent studies have focused on shoreline changes (Hedley et al., 2010; Anthony et al., 2019), flood risks and their impacts (Besset et al., 2017; Brakenridge et al., 2017), Holocene delta evolution (Giosan et al., 2018), geomorphological trends of the fluvial to marine transition zone for the Pathein River (which is the westernmost distributary of the Irrawaddy River) (Gugliotta and Saito, 2019), and sediment dispersal and accumulation on the shelf (Rodolfo, 1975; Rao et al., 2005; Kuehl et al., 2019; Liu et al., 2020). There is a gap of over 20 years between the two phases of study. Consequently, long-term hydrological data are very sparse, which has hindered more widespread understanding of the delta's evolution. Although these studies provided a preliminary sketch of the evolution of the Irrawaddy Delta, its current research status belies its scientific importance and complexity. A more comprehensive knowledge base is therefore required to better understand the delta's recent evolution.

To bridge the gap of the knowledge base on the Irrawaddy Delta, we systematically reviewed the scientific literature on the delta's evolution. Then, we explored the shoreline changes along over 400 km of coastline from the westernmost Pathein River to the easternmost Yangon River, and studied the evolution of fluvial and coastal geomorphology since 1974 (Fig. 1). We further evaluated the effects of anthropogenic and natural disturbances. This study aims to address the following three research questions:

(1) What is the recent evolution pattern of the Irrawaddy, including shoreline and channel evolution, and coastal geomorphology?
(2) What are the major human disturbances affecting the delta's evolution, and what are their effects?
(3) What are the possible trends of the delta's evolution based on the potential impacts of natural factors, such as climate change, sea level rise, and subsidence?

The rest of the paper is structured as follows. Section 2 explains the physiography and hydrology in the Irrawaddy Basin, and identifies the approximate topographic break in the Irrawaddy Delta. Section 3 summarizes the water and sediment contributions of tributaries and their distributions in the distributaries of the Irrawaddy River. Section 4 reviews previous studies on the evolution of the Irrawaddy Delta. Section 5 introduces the materials we used and our research methods. Section 6 displays our results with respect to four aspects: shoreline change, area change, fluvial geomorphology, and coastal geomorphology. Section 7 discusses the influencing factors of the delta evolution, including land use changes, dam construction, and sediment mining, provides a summary of current delta evolution. Section 8 provides our conclusions and recommendations.

2. Physiography and hydrology of the Irrawaddy River

The Irrawaddy River originates from the confluence of the N'mai and Mali Rivers in the glaciers of the southeastern Himalayas. It then flows to the southwest and combines with its western neighbor and largest tributary, the Chindwin River, in the middle of the Irrawaddy Basin. The three tributaries originate in high-rainfall regions, and thus generate approximately 60% of the total flow of the Upper Irrawaddy River. Other important tributaries include the Taping River, Shweli River, Myitnge River, and Mu River. The river continues to meander through the Central Dry Zone, and then flows through the container valley between Minbu and Pyay to enter the Irrawaddy Delta (Fig. 1). At the apex of the Irrawaddy Delta, located about 90 km north of Hinthada, the Irrawaddy River branches on the first order into the Pathein River in the west and the Myitmakha River, a tributary of the Yangon River, in the east (Figs. 1 and 2). Between Nyaungdon and Kywe Done, the river branches on the second order into four distributaries: the Pan Hlaing River, Toe River, Ya Zu Daing River, and Wakema River. Between the first and second order bifurcation points, there is an obvious meander belt with alluvial ridges along abandoned paleochannels and active channels, which is most conspicuous along the abandoned Daga River channel (Giosan et al., 2018) (Figs. 3 and 4). In the Lower Irrawaddy, many secondary branches anastomose to form a complex distributary channel network; this network finally ends in the shallow Andaman Sea, forming a lobate lower delta with eleven estuaries. Seven of the eleven major river mouths are located on the western delta coast.

The Irrawaddy Basin has a primarily tropical monsoon climate with distinct dry and rainy seasons. In the dry season, the northeast (NE) monsoon is active between November and February, while in the rainy season, the southwest (SW) monsoon is active between May and October. Although its mean annual precipitation varies widely from 500 mm to 4000 mm, the heaviest rains occur during the rainy season, accounting for 90% of the annual precipitation in the area (Furuichi et al., 2009). The heavy seasonal rain-induced floods carry enormous amounts of sediments into the coastal sea. Approximately 87% of the sediment discharged annually by the Irrawaddy River is delivered to the sea during the SW monsoon season. About 90% of the sediment is composed of suspended silt and clay and is transported eastward into the Gulf of Martaban by tidal and prevailing SW monsoon currents (Rodolfo, 1975; Rao et al., 2005). Only a minor portion of the Irrawaddy's load may be pushed by surface currents westward into the Bay of Bengal during the NE monsoon period (Rao et al., 2005, Liu et al., 2020). This forms a turbidity front oscillating approximately 150 km in phase with spring–neap tidal cycles in the central portion of the Gulf of Martaban (Ramaswamy et al., 2004).

The Irrawaddy Delta is a type of mud–silt semidiurnal tide-dominated system with a mean tidal range of 3 to 6 m (Brakenridge et al., 2017). The tidal range increases from west to east along the delta coast. However, most local tidal data were derived from studies conducted nearly half a century ago, and these data exhibit extreme levels of variability. Based on a collation of data by Kravtsova et al. (2009), the tidal ranges during the spring and neap tides west of the delta coast are 2.2 m and 1.8 m, whereas they are 5.7 m and 4.0 m at the eastern periphery of the delta coast, respectively. The Irrawaddy River mouths have a mesotidal range of 2 to 4 m, and the tidal range is between 4 and 7 m in the Gulf of Martaban (Ramaswamy et al., 2004). The spring tide's influence extends nearly 300 km inland to the apex of the delta area (Hedley et al., 2010). In the northern Andaman Sea, during the spring tide, the tidal current velocity reaches as high as 3 m/s, which leads to substantial sediment suspension and re-suspension, thus generating a perennial high-turbidity zone in the gulf (Ramaswamy et al., 2004). Recent geophysical survey indicated that the modern Irrawaddy River derived sediment has accumulated in the Gulf of Martaban with a rate of 215×10^6 tons/year and formed a 60-m-thick mud depocenter on the shelf (Liu et al., 2020).

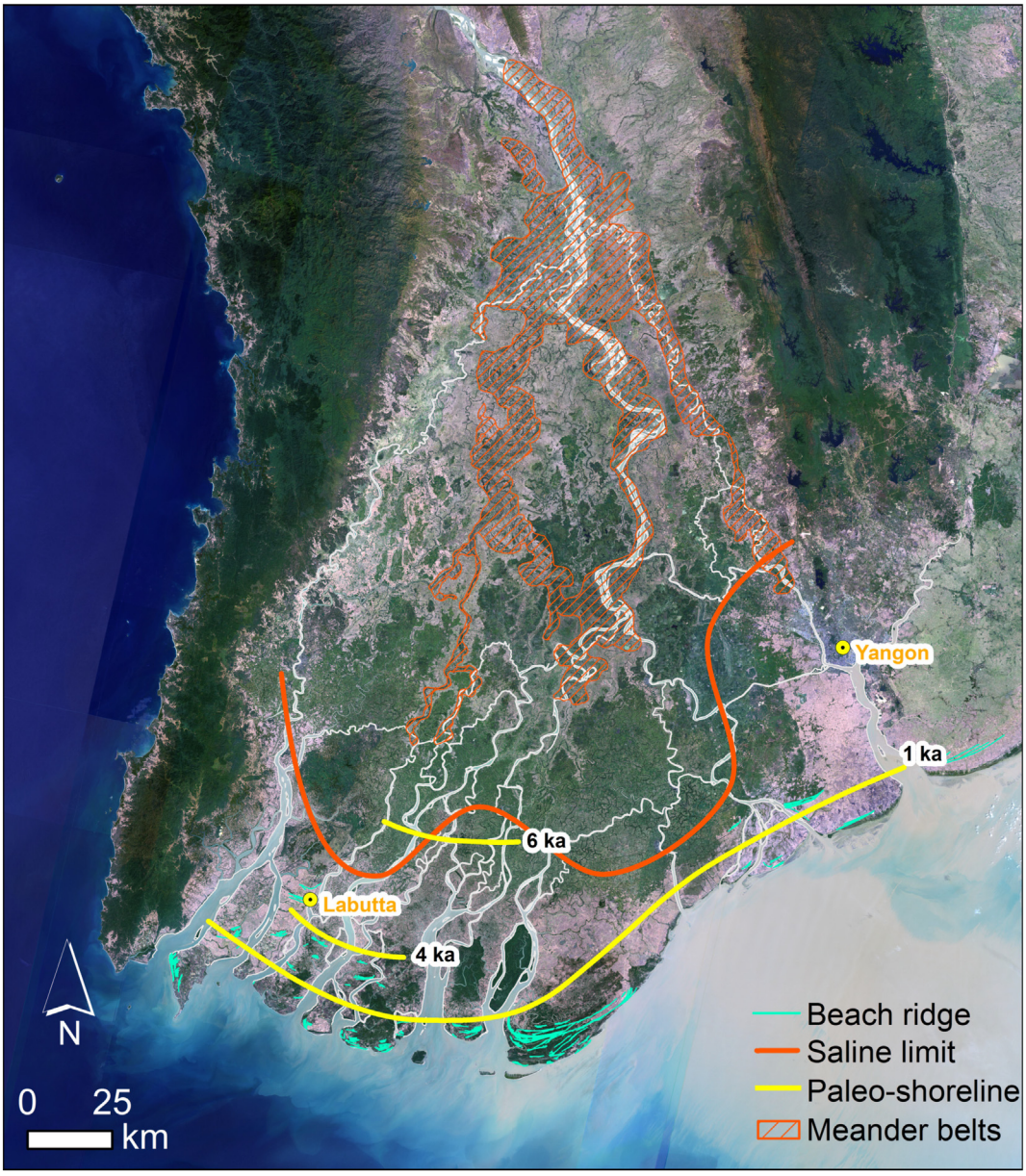

Fig. 3. Bifurcation configuration of the Irrawaddy in the delta. An obvious meander belt with alluvial ridges is present along abandoned paleochannels and active channels between the first- and second-order bifurcation points. The beach ridges were mainly distributed within the interdistributary plain of the lowermost delta (Kravtsova et al., 2009; Giosan et al., 2018). The paleo-shoreline position was adopted from Giosan et al. (2018). The underlying images are based on Landsat 8 Operational Land Imager (OLI) data recorded in 2018.

3. Water and sediment discharge from the Irrawaddy and its distributaries

The Irrawaddy River plays a major role in global sediment budgets, although the existing sediment data remain controversial (Hennig, 2016). The Irrawaddy and Salween basin systems are estimated to have contributed approximately 20% of the total mass flux into the sea for all rivers originating from the Himalayan Tibetan Plateau orogenic belt (Milliman and Meade, 1983). The original sediment flux data came from Gordon (1879), who reported that the average annual sediment load for 10 years (1869–1879) was 286×10^6 tons/year. Milliman and Meade (1983) provided a similar figure of 285×10^6 tons/year. However, Gordon (1885) reduced the estimation of the flux to 261×10^6 tons/year, which is now the most commonly quoted value. Robinson et al. (2007) re-analyzed the original data of Gordon (1879) and considered that the often-quoted flux value was underestimated by 27%; they reported that the true annual Irrawaddy suspended sediment load was as much as $364 \pm 60 \times 10^6$ tons, and the annual average water discharge was estimated to be between $422 \pm 41 \times 10^9$ m^3 and $440 \pm 48 \times 10^9$ m^3, which is comparable to Gordon's (1879–1880) value of 425×10^9 m^3/year and Milliman's value of 428×10^9 m^3/year. Given that the sediment loads from Chinese rivers have been greatly reduced because of dam construction, the new flux value would make the Irrawaddy River the third-largest contributor of global sediment budgets (Robinson et al., 2007). Based on the data collected from 1969 to 1996 at Pyay, 60 km upstream of the Irrawaddy Delta head, Furuichi et al. (2009) estimated modern water discharge to be $379 \pm 47 \times 10^9$ m^3/year and the sediment load to be $325 \pm 57 \times 10^6$ tons/year. Furuichi et al. (2009) also stated that the discharge has significantly decreased over the last 100 years.

At the first-order bifurcation point, minimal water was historically diverted into the Pathein and Myitmakha Rivers (Stamp, 1940). An

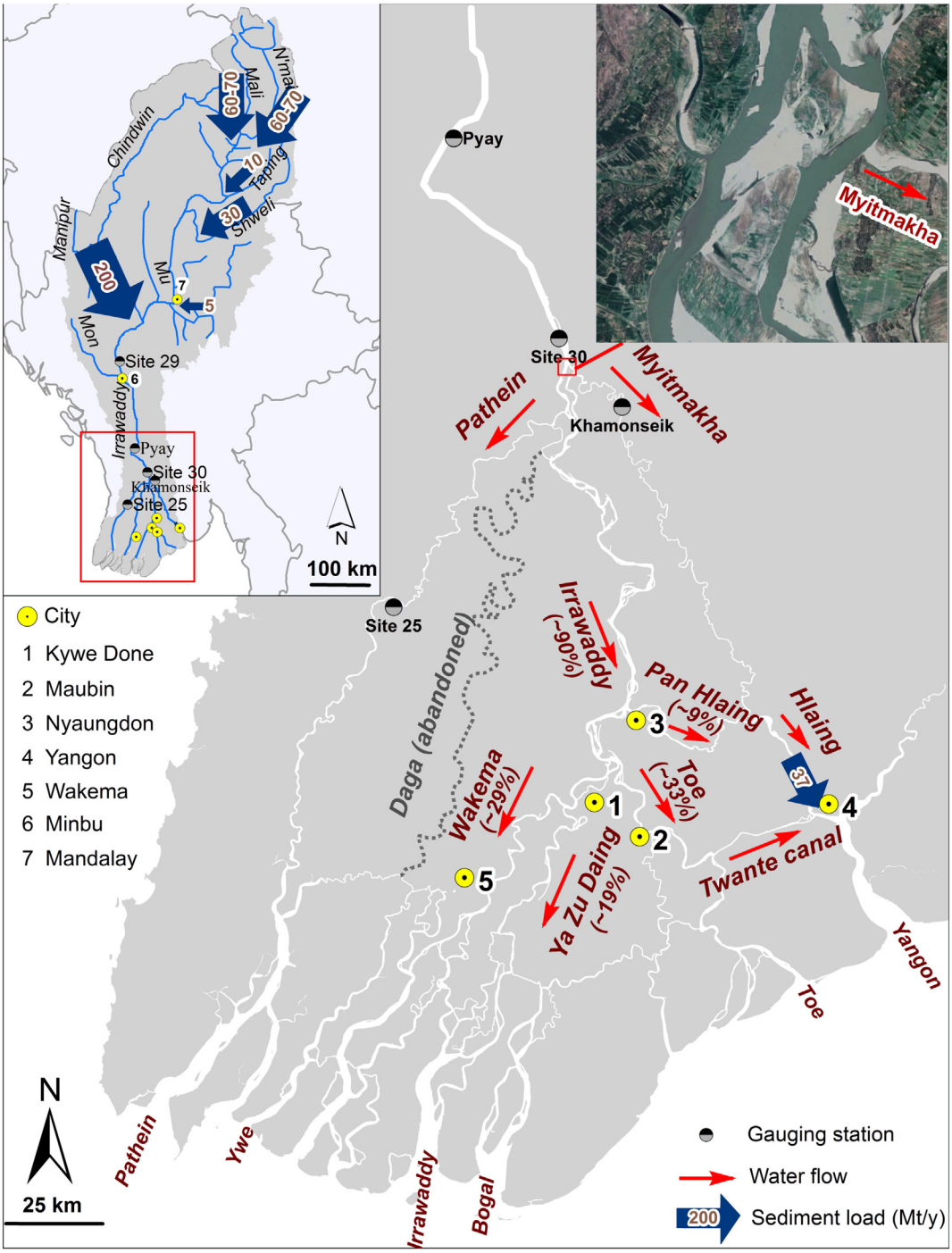

Fig. 4. Water and sediment contributions of tributaries and their distributions in the distributaries of the Irrawaddy River (based on Halcrow, 1982; Brichieri-Columbi, 1983; Kravtsova et al., 2009; Garzanti et al., 2016). The Google Earth image captured in 2018 clearly shows that the bifurcation mouth into the Myitmakha River is clogged during the low-flow season.

earlier estimation showed that the two distributaries can share 15% discharge in the flood season (Halcrow, 1982). According to remotely monitored data from River and Reservoir Watch Version 3.5 (Brakenridge and Kettner, 2018), Site 29 (below the confluence of the Chindwin River) and Site 30 (just above the first-order bifurcation point) recorded very similar average discharges of 334×10^9 m^3/year and 328×10^9 m^3/year, respectively, from 1998 to 2018; however, Site 25 in the Pathein River below the first-order bifurcation point showed a discharge of only 8×10^9 m^3/year (Fig. 4). The average discharge at Khamonseik station in the Myitmakha River below the first-order bifurcation point was 19×10^9 m^3/year from 1987 to 2000 (JICA and YCDC, 2002) (Fig. 4). We can also clearly observe from satellite images that the bifurcation mouth into the Myitmakha River is clogged during the low-flow season (Fig. 4); therefore, only a very small amount of water within the Irrawaddy's mainstream can flow into the Myitmakha River. Thus, we estimated that the Irrawaddy mainstream may carry over 90% of the discharge passing its first-order bifurcation point. At the second-order bifurcation point, according to Brichieri-Columbi (1983) and Kravtsova et al. (2009), the four distributaries of Pan Hlaing, Toe, Ya Zu Daing, and Wakema receive 10%, 37%, 21%, and

32% of discharge from the Irrawaddy mainstream, respectively (Fig. 4). As a result, the Irrawaddy, Bogale, and Toe distributaries may be the main channels of water and sediment discharges into the sea from the Irrawaddy mainstream, and only their mouth bars are most developed along the delta coast.

Based on Gordon's value, Stamp (1940) estimated that 32×10^6 tons/year of sediment was transported at Mandalay, 109×10^6 tons/year came from the Chindwin River, and 120×10^6 tons/year was contributed by the non-perennial streams in the Central Dry Zone, accounting for 12%, 42%, and 46% of the total load, respectively. Based on geochemical data and a total annual sediment load of $350–400 \times 10^6$ tons, Garzanti et al. (2016) calculated that approximately 200×10^6 tons (~53%) came from the Chindwin, whereas the headwater rivers of N'mai and Mali contributed $60–70 \times 10^6$ tons (collectively ~35%), and other tributaries including the Taping, Shweli, and Myitnge contributed the remaining 45×10^6 tons (~12%). These proportions are higher than those reported by Stamp (1940). For the lower delta, Halcrow (1982) estimated that the Hlaing River, Panhlaing Creek, and the Twante Canal together brought 37×10^6 tons of sediment annually (Fig. 4).

4. Previous studies on the evolution of the Irrawaddy Delta

The bulk of the sediment load from the Irrawaddy during annual flooding is brought out to the Gulf of Martaban (Rao et al., 2005), with very little coarse sediment left to sustain the slow growth of the delta shoreline (Rodolfo, 1975). Alluvial ridge construction within the meander belt suggests a fluvial-dominated environment in the upper delta (Giosan et al., 2018). The ridges fade out as the trunk channels start to bifurcate into distributaries in the mid-delta, and beach ridges resulting from wave action occur along the contemporary coasts of the lower delta (Fig. 3). Wave-built beach ridge construction during the late Holocene is a common feature in some deltas across the Indian monsoon region, such as in the Red River (Tanabe et al., 2006), Mekong (Tamura et al., 2012), Chao Phraya (Tanabe et al., 2003), and Subarnarekha (Maiti, 2013) deltas. In contrast, the beach ridges are generally underdeveloped in the Irrawaddy Delta. These shore-parallel beach ridges that coalesce into beach-ridge plains are mainly located on the coasts in the Bogale lobe, in which the maximum beach ridge sequence extends over 20 km. The oldest beach ridge bundle found on the western side of the delta near Labutta is estimated to have formed approximately 4600 years ago, and the beach ridge plain at the Bogale lobe began to form approximately 1000 years ago (Giosan et al., 2018) (Fig. 3).

The earlier estimations of the delta advance rate present large variability, probably because of the differences between the study area and the dataset used. Chhibber (1934) estimated that the delta advanced at a rate of 48 m/year based on surveys from 1860–1870 and 1909–1910. Rodolfo (1975) reported an average shoreline growth rate of 25 m/year based on more recent data. Kravtsova et al. (2009) offered a progradation rate of 50–60 m/year. However, Hedley et al. (2010) posited that the delta shoreline (including the Sittang River mouth) remained largely unchanged from 1850 to 2006 despite abundant amounts of sediment debouched annually into the coastal sea. The shoreline has advanced at a rate of no >3.4 m/year, and the average area increase rate has been 4.2 km^2/year since 1925. During this period, rapid accumulation occurred at a rate of 8.7 km^2/year from 1925 to 1989, and the net erosion rate was 13 km^2/year from 1989 to 2006. Accordingly, Hedley et al. (2010) concluded that sediment deposition balances subsidence and sea-level rise in the delta, meaning that the delta shoreline is generally in equilibrium. Besset et al. (2017) revealed that considerable erosion occurred in the Irrawaddy Delta during and after Tropical Cyclone Nargis (2008). Giosan et al. (2018) provided a first look at the evolution of the Irrawaddy Delta during the Holocene, thereby laying the groundwork for further research. Anthony et al. (2019) studied the shoreline change from 1974 to 2019 in the delta and found that 49% of the shoreline was eroded with an overall shoreline change rate of approximately 9.5 m/year. In addition, they considered that reduced riverine sediment supply induced by dams and in-channel sediment mining caused the erosion. Recent offshore geochemical and geophysical studies indicated that there is a little Irrawaddy-derived sediment accumulated near its current river mouths, instead, majority of them are transported eastward in the Gulf of Martaban, some drift westward and northward into the Bay of Bengal (Kuehl et al., 2019; Liu et al., 2020). These studies provide a preliminary sketch of the evolution of the Irrawaddy Delta and sediment transport features along its delta front.

5. Materials and methods

5.1. Data collection

The data used in this paper mainly include those on water and sediment discharge, digital shoreline, fluvial and coastal geomorphology, land use change, hydropower, and irrigation dam. The relevant literature, satellite images, and online data were our main data sources. The water and sediment discharge data were obtained from some literature sources mentioned in Section 3, and the remotely monitored data were obtained from River and Reservoir Watch Version 3.5 (Brakenridge and Kettner, 2018). The fluvial and coastal geomorphology was visually interpreted from Landsat images and Google Earth high-resolution images. For example, the meander belts were identified from Google Earth images by referring to Giosan et al. (2018), and the beach ridges were manually delineated from the Landsat images (Fig. 3). The deforestation data were acquired from the Hansen Global Forest Change v1.6 (2000–2018) dataset released in the Google Earth Engine (GEE) platform by Hansen et al. (2013) and other literature mentioned in Section 7.1.1. The terrestrial mining data were mainly procured from LaJeunesse Connette et al. (2016) and downloaded from the GeoNode website, an open source platform for sharing geospatial data and maps (http://geonode.themimu.info/layers/geonode%3Amining_areas). The aquaculture, hydropower dam, and irrigation reservoir data were derived from publications presented in Sections 7.1.1, 7.1.2 and our remote-sensing interpretation. The wind data used in Fig. 20 were retrieved from http://earth.nullschool.net/.

5.2. Shoreline interpretation and analysis

The shoreline is one of the 27 geographical features recognized by the International Geographic Data Commission (Colin et al., 2001), and shoreline change analysis has become a useful tool to evaluate delta evolution (Anthony et al., 2015; Li et al., 2017). The shoreline is a highly dynamic feature and not a truly fixed line; some shoreline indicators are commonly used as a proxy to represent the “true” shoreline position (Boak and Turner, 2005). The Irrawaddy Delta coast is dominated by mangrove forests (Webb et al., 2014), and mangroves are considered to be the best geological indicators in global shoreline change research (Souza et al., 2006); therefore, the vegetation line was used as the proxy shoreline in this study. However, mangroves are mainly distributed along parts of the delta coast, and some parts of the coast and the distributary channel shoreline cannot be covered. In addition, vegetation growth has seasonal and annual variations. To more accurately depict the shoreline changes and avoid the influences of tidal level and cloud coverage as much as possible, we first calculated the annual maximum normalized difference vegetation index (NDVI) based on all available Landsat image datasets in the GEE platform (Gorelick et al., 2017). The NDVI was selected to extract the shorelines of the delta and channels for the following nine years, 1974, 1978, 1988, 1993, 1998, 2003, 2008, 2013, and 2018, because the spectral curves of vegetation and water in the near-infrared and red bands are obviously different (Li and Gong, 2016). Then, a threshold method was used to obtain the digital shorelines (Fig. 5). Finally, the digital shorelines were modified manually by referring to the original pseudocolor composite image.

To reduce the digitalization error as much as possible, the entire process was completed by the same person. Finally, we extracted the shorelines of channel banks, channel bars, the delta front, and mouth bars in the delta (Fig. 6). The shoreline change rate was calculated for the delta front, and the area change was derived for all parts.

We used the DSAS tool to analyze shoreline change of the delta front in the Irrawaddy Delta. A total of 1552 transects were generated from west to east along the over 400-km coast. We adopted two methods provided by DSAS to calculate the shoreline change rate. One was the linear regression rate (LRR) method, which was used to compute the total shoreline change rate from 1974 to 2018. The LRR was determined by fitting a least-squares regression line to all points of intersection between shorelines and a specific transect (Thieler et al., 2017). As all shorelines can be considered, the LRR is considered the most robust quantitative method to evaluate the shoreline change rate (Morton and Miller, 2005; Addo et al., 2008) and has the advantage of reducing short-term variability and potential random errors (Maiti and Bhattacharya, 2009). Positive and negative LRR values represented the states of accretion and erosion, respectively. The other method was the end point rate (EPR), which was used to derive the temporal trend of the shoreline change rate. The EPR was first computed for every two adjacent years for every transect. Then, the temporal trend of the shoreline change rate could be obtained for each transect.

We further calculated the net area changes at different azimuthal angles based on the shorelines in 1974 and 2018 and the transects. We first assigned an accretion or erosion attribute and a corresponding

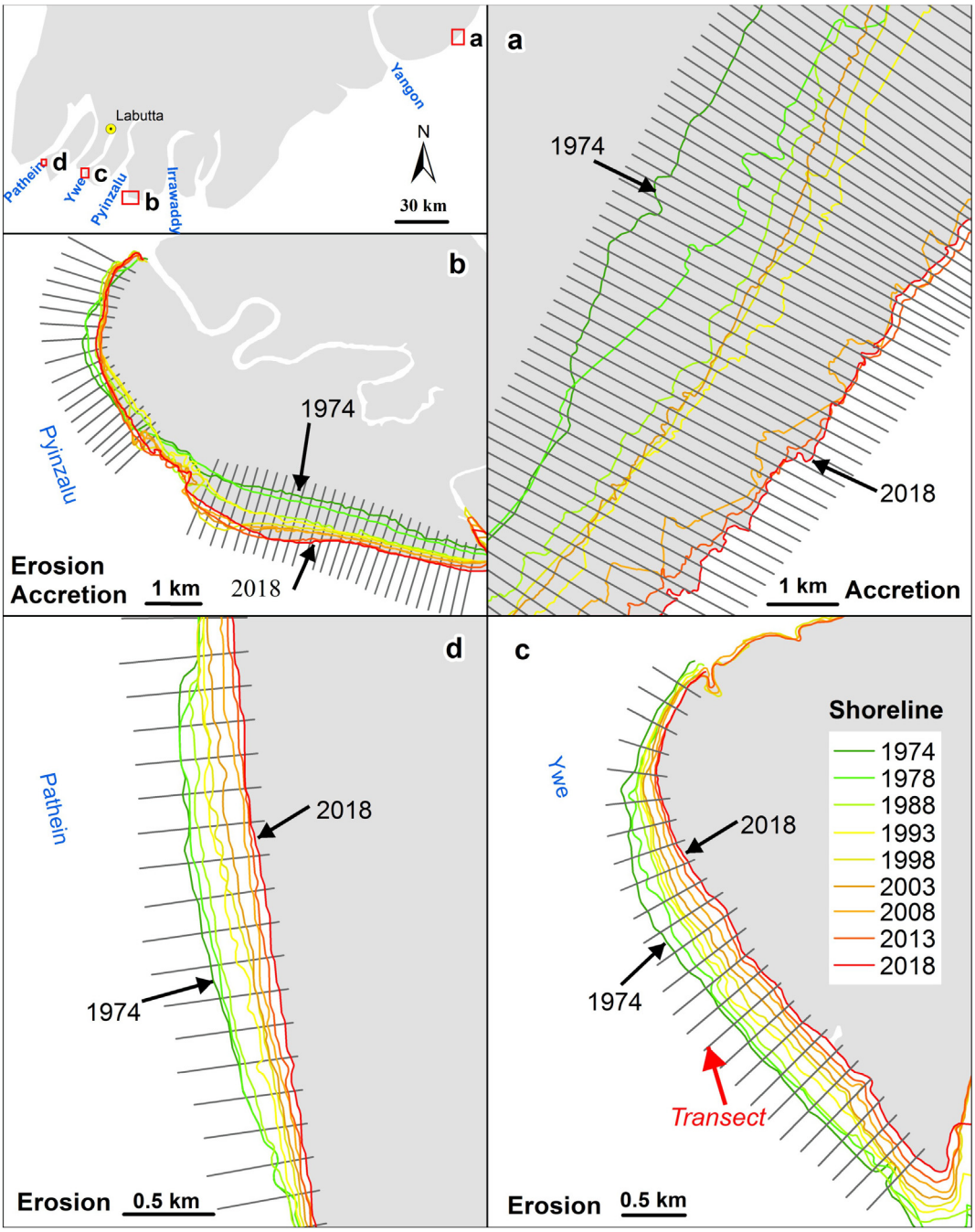

Fig. 5. Selected locations showing detailed shoreline changes derived from Landsat images during 1974 to 2018.

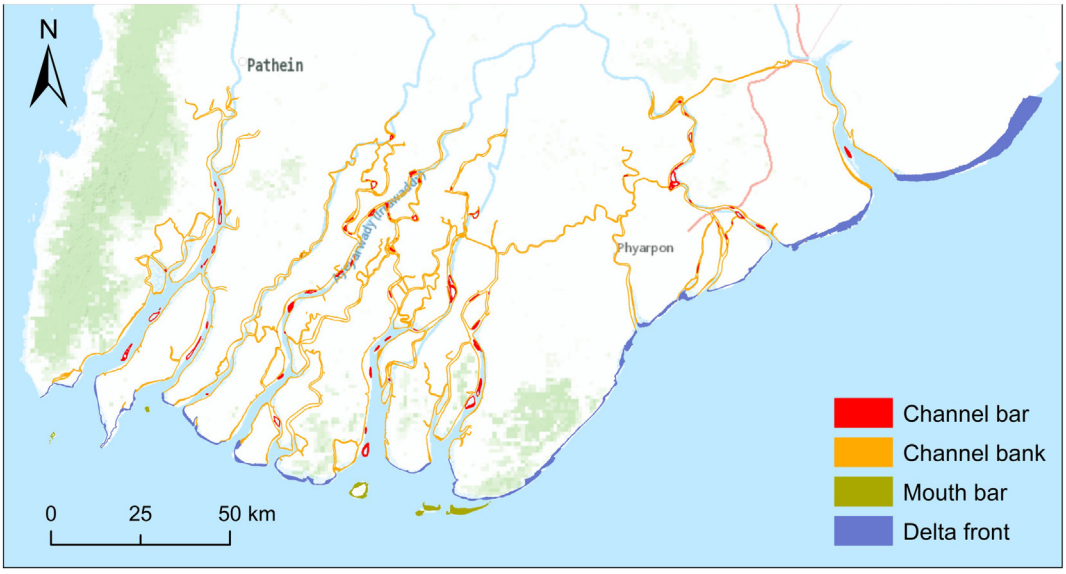

Fig. 6. Evolution of the Irrawaddy Delta as represented by four geographical features: channel bar, channel bank, mouth bar, and delta front.

orientation to each part defined by each two neighboring transects and the shorelines in 1974 and 2018, and calculated its net area change along the delta coast. We then divided 360 degrees into 16 equal intervals, namely, 16 orientations. Finally, we classified all the parts along the delta coast into these 16 orientations. Thus, we derived the net area changes at different azimuthal angles, which were associated with the prevailing monsoon direction.

5.3. Remote sensing-derived shoreline uncertainty

Landsat images have been successfully used to monitor the dynamics of shorelines, including even subtle variations with sub-pixel accuracy (Li and Gong, 2016; Hagenaars et al., 2018). For example, Muslim et al. (2007) obtained shoreline positional accuracy of <2 m using Landsat images, and Pardo-Pascual et al. (2012, 2018) concluded that the mean horizontal error of shorelines detected from successive Landsat TM and ETM+ images is close 5 m. In general, the spatial location of the shoreline is affected by many factors, including vegetation growth, typhoons, storms, and rectification of remote sensing images. According to Romine et al. (2009), shoreline positional errors include five aspects with regard to remote-sensing-derived shorelines: digitization, pixel, seasonal, rectification, and tidal errors. The Irrawaddy Delta is a typical large tropical delta, where mangroves with a certain height are widely distributed along the delta coast, and the annual maximum NDVI method will reduce the negative effects of seasonality to the minimum extent. This means that tidal fluctuation and seasonal variability have little impact on the shoreline position (Phan et al., 2015). The rectification error can be acquired from the metadata file of the Landsat image or by a geometric correction procedure (<0.5 pixels or 15–30 m). For Landsat images, the pixel error can be incorporated into the rectification error. The digitization error can be defined as the standard deviation in shoreline positions from repeated digitization by a single operator, and the error was <0.5 pixels (Fletcher et al., 2012; Li et al., 2014). However, the early Landsat Multispectral Scanner (MSS) images with lower resolution of 60 m may increase the uncertainty of the results in the corresponding time period. In addition, the LRR method will reduce potential random errors (Maiti and Bhattacharya, 2009), and shoreline positional error can also be alleviated by increasing the length of the study periods (Morton et al., 2004). Finally, the mangrove shoreline is extremely sensitive to sediment yield, erosion and deposition processes, climate change, and human intervention (Kuenzer et al., 2011; Alongi, 2015), and mangroves are considered to be the best geological indicator in global shoreline change research (Souza et al., 2006). Therefore, the shoreline change calculated in this study represents a comprehensive response to many natural and anthropogenic factors that determine the accretion or erosion of the delta coast (Shearman et al., 2013).

6. Results

6.1. Shoreline change along the delta front

In general, of the total shoreline length, accreted and eroded shorelines accounted for 58% and 42%, respectively, during 1974–2018 (Fig. 7). The maximum and average accretion (erosion) rates of the accreted (eroded) areas were 98.8 m/year (−19.3 m/year) and 21.4 m/year (−4.7 m/year), respectively. The overall average shoreline change rate was 10.4 m/year. The shoreline change rate gradually increased from west to east along the delta coast. Erosion was dominant in the western multi-channel estuary area, and accretion was mainly located on the eastern coast.

Based on the average shoreline change rate along the coast (Fig. 7a), the delta coast can be obviously divided into two parts, the western eroded coast and the eastern accreted coast, and each area can be further divided into two parts, ultimately comprising a total of four zones (Fig. 7b). Zone 1 includes the area from the Pathein estuary to the Thetkethaung estuary; Zone 2 spans from the Ywe estuary to the west side of Pyapon estuary; Zone 3 extends from the west side of Pyapon estuary to the Toe estuary; and Zone 4 includes east of the Toe estuary, mainly consisting of both sides of the Yangon estuary. Zone 1 and Zone 2 cover the west multi-channel estuaries, belonging to the erosional coast, and Zone 3 and Zone 4 cover most of the east coast in the Irrawaddy Delta with visible accretion characteristics, with 81% of the shoreline accreting. Although Zone 1 and Zone 2 together barely had a positive value (0.1 m/year) in the average shoreline change rate, erosion occupied 60% of the shoreline length, and most of the accretion was derived from the growth of spits along the coast. Thus, the western coast showed erosional tendencies overall. Both the western and eastern coasts did not present significant trends in the shoreline change rate. However, interestingly, the fluctuations in the shoreline change rates were almost opposite for the two parts (Fig. 7d). On the western coast, the maximum accretion rate of 5.0 m/year occurred from 2008

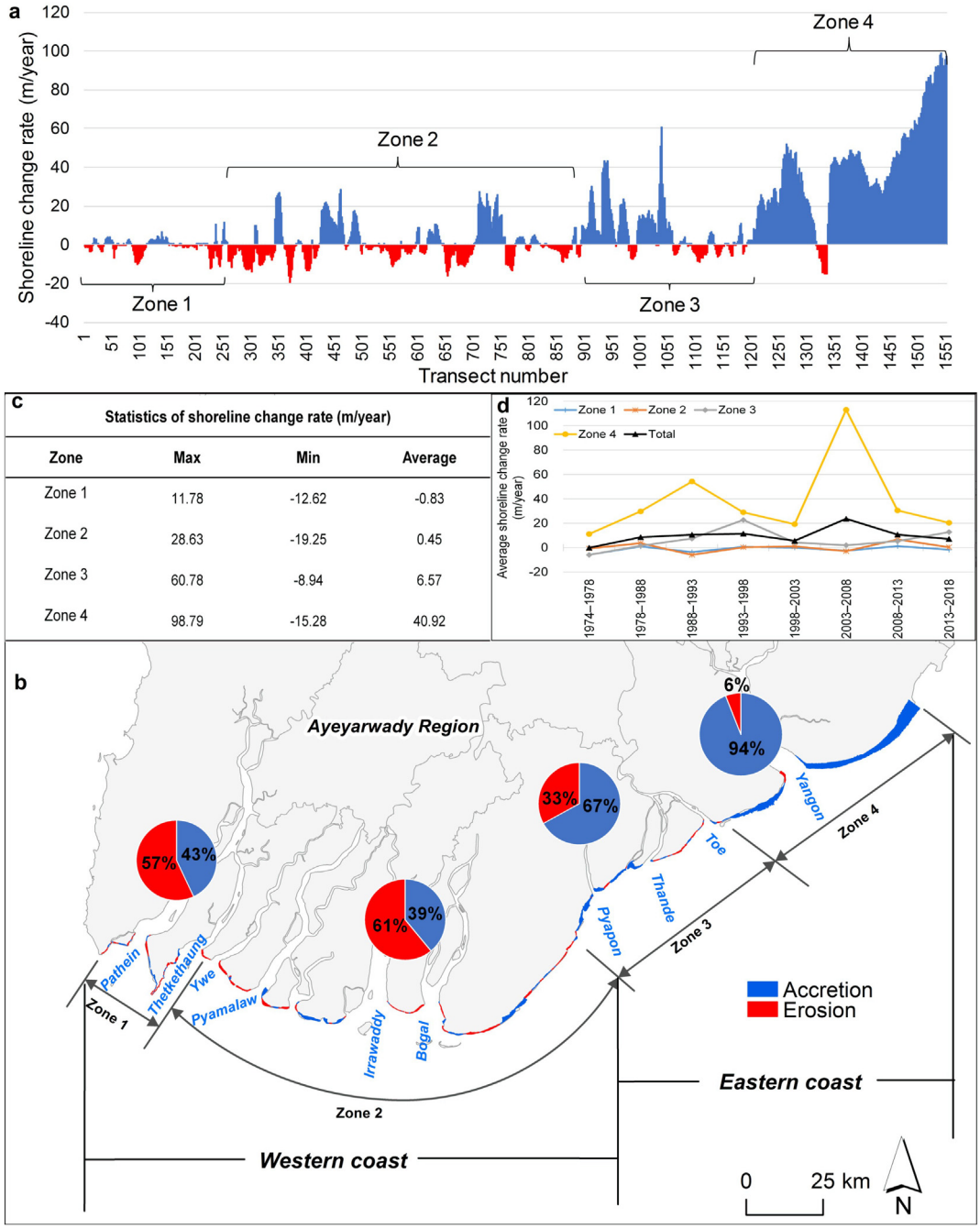

Fig. 7. (a) According to the average shoreline change rates, the delta coast was divided into four parts: Zone 1, Zone 2, Zone 3, and Zone 4; (b) pie charts show the proportions of the shoreline length of erosion and accretion in each zone; (c) table displays the maximum, minimum, and average shoreline change rates of the four zones; (d) line graph shows the average shoreline change rates for the four zones over time. The transects are numbered from west to east along the coast of the Irrawaddy Delta. Positive and negative values indicate accretion and erosion, respectively.

to 2013, whereas the maximum erosion rate of −5.3 m/year occurred from 1988 to 1993. On the eastern coast, the maximum accretion rate of 58.2 m/year occurred from 2003 to 2008.

Furthermore, based on the shoreline change rates and changes in the shoreline change rates of two adjacent years, the shoreline changes in the delta front of the Irrawaddy Delta can be divided into four states (Fig. 8): increasing accretion, decreasing accretion, increasing erosion, and decreasing erosion. Zones 1 and 2 showed large proportions of increasing erosion, at 32% and 31%, respectively; erosion on the coasts of the Ka Don Ka Ni village tract (over 14 km long) and from the central coast of the Kone Gyi village tract to the Thetkethaung estuary (nearly 24 km long) almost exclusively comprised the shoreline changes in these zones, and over 60% of the shorelines in these areas were in a state of increasing erosion. Zones 3 and 4 showed large proportions of increasing accretion, at 42% and 63%, respectively. The accretion was mainly located on both sides of the Pyapon estuary at the concave coast, whereas erosion in these areas mainly occurred between the Thande and Toe estuaries on the convex coast in Zone 3. The proportions of both increasing and decreasing erosion together made up for only 3% in Zone 4, thereby indicating that the delta coast on both sides of the Yangon estuary will likely continue to expand into the sea in the near future.

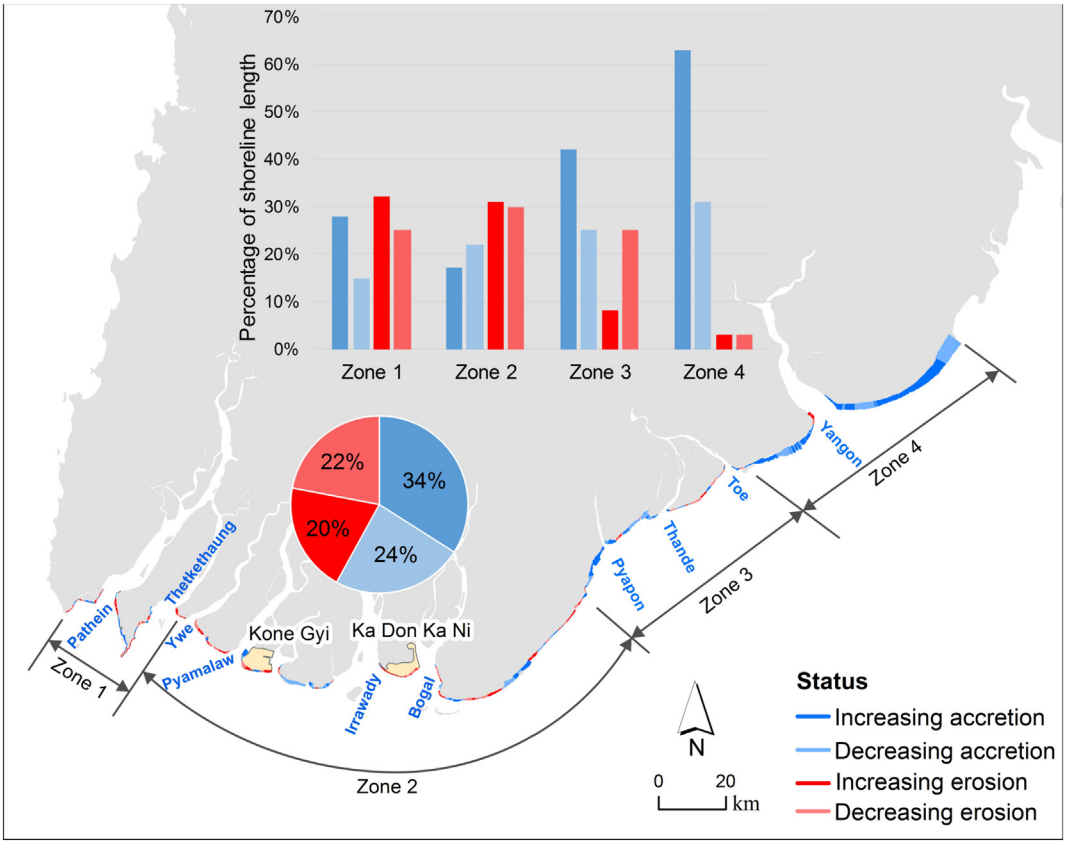

Fig. 8. The Irrawaddy shoreline can be divided into four categories: increasing accretion, decreasing accretion, increasing erosion, and decreasing erosion. The bar chart shows the proportions of the four types of statuses to shoreline lengths in each zone, and the pie chart represents the proportions of each type of status to the overall shoreline length.

6.2. Area change along the delta front and channels

To explore the spatial pattern of the evolution of the Irrawaddy Delta, we extended the four zones shown in Fig. 7 inland to include the channels. Thus, the Pathein River was assigned to Zone 1; the Ywe, Pyamalaw, Irrawaddy, and Bogale Rivers were assigned to Zone 2; the Thande River was assigned to Zone 3; and the Yangon River was assigned to Zone 4. The net area gain was 194.0 km^2 in the study area from 1974 to 2018; among this net gain, the channel bar, channel bank, mouth bar, and delta front changes contributed 11%, 5%, 8%, and 76%, respectively. The channel bar and mouth bar changes mainly came from Zone 2; Zone 1 contributed most of the area gain for channel bank changes, whereas the channel bank in Zone 2 had a large spatial adjustment but a smaller area increase; the area change for the delta front mainly occurred in Zone 4. Erosion was mainly distributed along the western delta front, and was also conspicuous in two estuarine reaches of distributary mouths: a 45-km estuarine reach of the Irrawaddy channel and a 40-km reach below the confluence of the Yangon River (Fig. 9). The channels in Zone 2 are highly active because of channel avulsion and growth of channel bars in the middle part of the study area. The accretion and erosion areas were closely aligned at 65.8 km^2 and 63.0 km^2, respectively, for the channel banks in Zone 2. The area for channel bars showed a net increase of 22.0 km^2 throughout the study area; over 70% of this increase came from Zone 2, but the channel bars were largely eroded in the estuarine reach. The mouth bars were also mainly located in Zone 2, thereby representing a net increase of 14.2 km^2. The delta front showed a net increase of 128.9 km^2 in Zone 4.

Overall, the area change rates did not present obvious trends for all four types of geographical features. The large fluctuations over several time intervals were likely the results of extreme events. Moreover, the mouth bar change is an exception whose area showed a significant increase as the sandbars became large and moved toward the coast. However, the western and eastern parts displayed distinctive characteristics in the study area (Fig. 10a). Zone 2 accounted for a large share of the area change in the western part during the study period; additionally, the channel banks, channel bars, and mouth bars, except for the delta front, showed substantial changes in Zone 2. For the channel banks, the area change rate fluctuated widely between −3.4 km^2/year and 2.1 km^2/year before 1993 but has fluctuated only slightly, near zero, since then as a result of the accretion and erosion mostly compensating for each other. On channel bars, accretion has dominated since 1974, and the accretion rate exhibited a U-shaped change. The maximum accretion rate of 0.81 km^2/year occurred from 1978 to 1988; the rate then reduced to 0.37 km^2/year from 1998 to 2003, and later rose to 0.59 km^2/year from 2013 to 2018. Mouth bars experienced a general growing trend (Fig. 10b). Their accretion rate reached a maximum of 0.78 km^2/year from 2003 to 2008 and from 2013 to 2018. However, it fell back to 0.48 km^2/year from 2008 to 2013 and was level from 1998 to 2003 (Fig. 11c). The area change in the eastern part of the study area was mainly derived from Zone 4, in which the delta front contributed the most accretion. The delta front became an obvious accretionary coast since 1974. The accretion rate showed minimal changes with an average of 2.4 km^2/year, except for a minimum of 0.2 km^2/year from 1998 to 2003 and a subsequent maximum of 9.4 km^2/year from 2003 to 2008 (Fig. 11d). The channel banks have generally eroded since 1974, apart from a weak accretion period at a rate of 0.07 km^2/year from 2008 to 2013 (Fig. 11a).

6.3. Evolution of fluvial geomorphology

As observed in the satellite images from 1974 to 2018 (Fig. 12), geomorphological changes were highly active at the two bifurcation points.

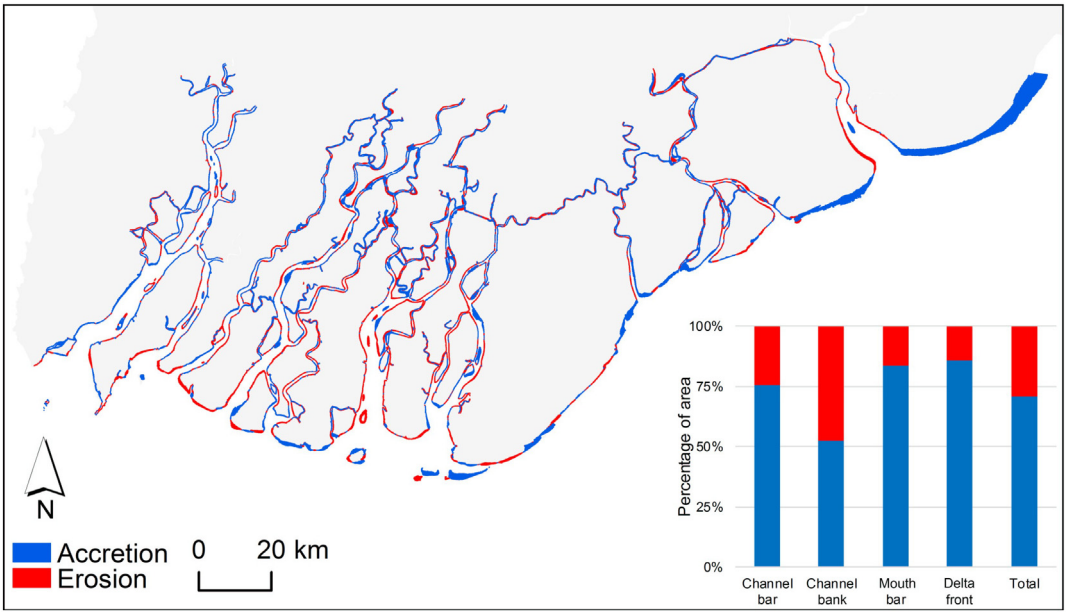

Fig. 9. Accretion and erosion changes in the Irrawaddy Delta from 1974 to 2018. The bar chart shows the percentages of area for the four types of geographical features and the entire study area.

At the first-order bifurcation point, the changes mainly manifested as more braided, less sinuous, widening channels, and increasing bifurcation angles. The main water course also moved approximately 2 km westwards to the side of Pathein River from 1974 to 2018; at the same time, the bifurcation mouth of the Pathein moved almost 20 km downstream. At the second-order bifurcation point, the observed geomorphological changes primarily included a less braided and more sinuous shape and increasing bifurcation angles. The distributary channels near the bifurcation mouths also became smoother over time. These changes in the two bifurcation points may have caused the ratio changes for water diversion into the distributaries.

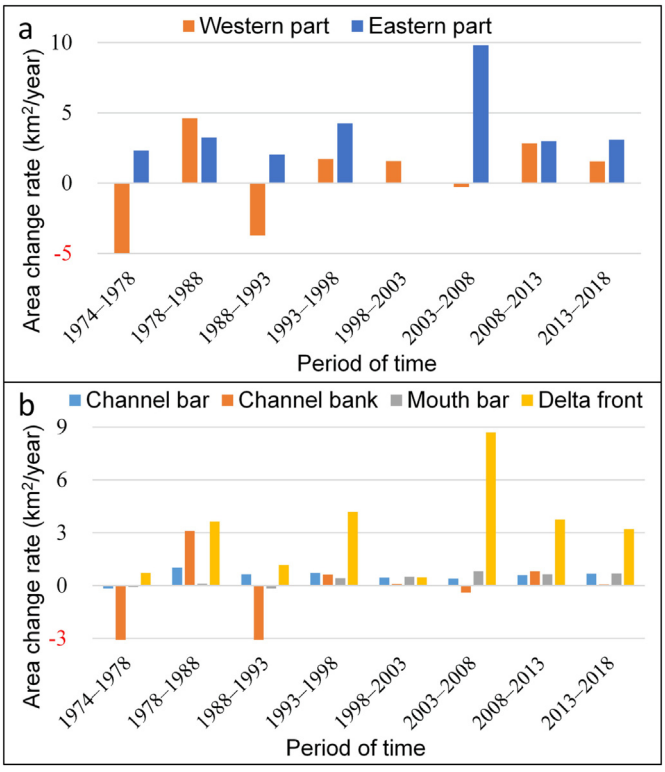

Fig. 10. Area change rates of the western and eastern parts (a), and the four types of geographical features (b) of the study area over different periods. In general, the area change rates did not present an obvious trend for all four types of geographical features; extreme events may have caused large fluctuations.

The upper part of the Irrawaddy Delta is characterized by a fluvial plain with a meander belt and active braided channel, which was mainly distributed upstream from the second-order bifurcation point. The lower part is the coastal delta plain, on which the braided channel gradually becomes an anastomosing channel with interdistributary plains and channel bars (Kravtsova et al., 2009; Giosan et al., 2018). The approximate topographic break, showing the boundary between the fluvial plain and coastal delta plain, can be identified near the second-order bifurcation point (Fig. 2). The reaches largely at the center of the study area for area change (Fig. 9) have experienced considerable channel adjustments, including sandbars merging with the channel bank, abandonment of small channels, and accretion and erosion of channel banks. Some small-scale but visible channel migrations occurred in the tributaries' upstream confluence of the Yangon River. The channel banks of the estuary reach were attributed to net erosion for all distributary channels except for the Pathein. However, the channel bars showed net accretion except for those in the Irrawaddy channel (Fig. 13a). The channels become stable and gradually straighten and widen downstream toward the estuaries. For the westernmost Pathein channel, the onset point of widening was identified at 100 km upstream of its river mouth (Gugliotta and Saito, 2019). Notably, the onset widening positions tend to move downstream for the distributary channels from west to east.

The sandbars have distinctive characteristics in the distributary channels of the lower delta. The westernmost Pathein and Thetkethaung channels have the largest numbers of sandbars with prevailing growth (Fig. 13b). More than a dozen sandbars can be observed in the channels from recent satellite images, and these sandbars are located near the channel centerline. The Ywe River had a small sandbar before 1998, but it has been eroded away completely. The river has relatively high sinuosity. Its upper reach was linked with the abandoned Daga River (circa the 1700s), which used to be the main river channel of the Irrawaddy (Syvitski et al., 2012; Giosan et al., 2018). The Pyamalaw River is a larger

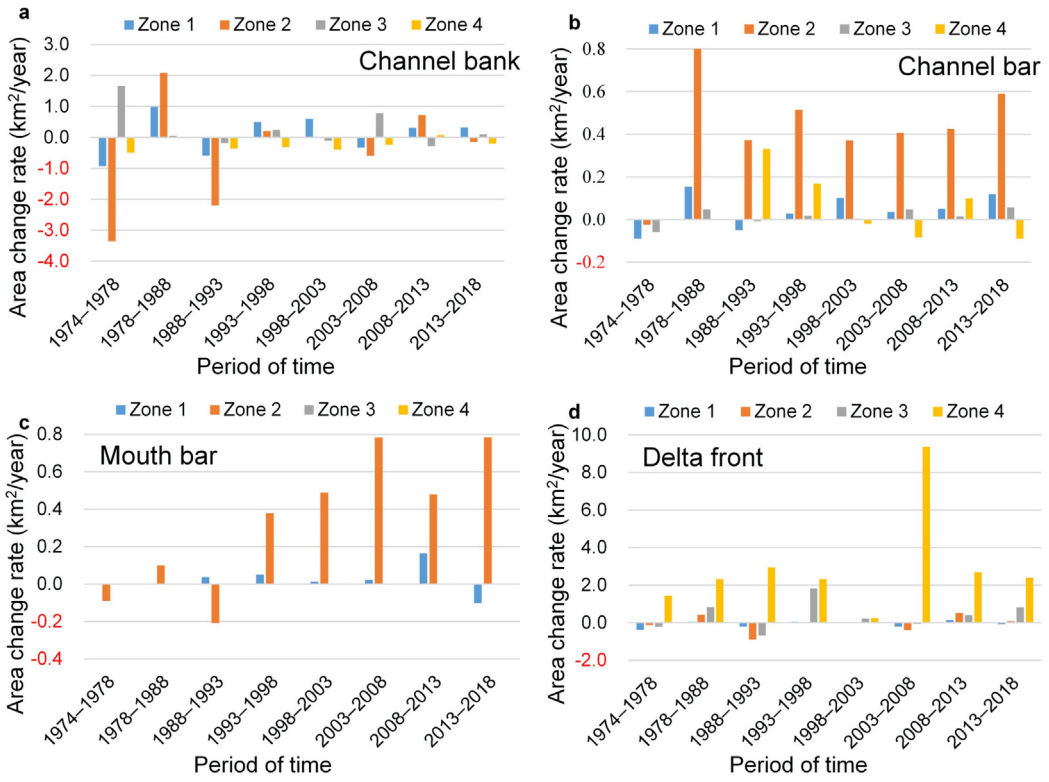

Fig. 11. Area change rates of channel banks, channel bars, mouth bars, and the delta front in the Irrawaddy Delta.

distributary. A few of the sandbars were progressively accreted adjacent to the channel bank, and widely distributed in the deflection, bifurcation, and confluence regions. The Irrawaddy is the largest channel flowing into the sea; its sandbars were mostly located near the channel centerline. These sandbars are notably eroded, and several have almost or even completely disappeared along the 30 km estuary reach. However, sandbars upstream showed accretion. The sandbars in the Bogale River also showed accretion, occurring at a position similar to those in the Pyamalaw River. The Pyapon River is a small distributary, and its only sandbar has merged into the channel bank. The sandbars tend to move downstream in the Thande and Toe rivers. The Yangon River has emergent sandbars with a lower variation found 10 km from its mouth.

6.4. Evolution of coastal geomorphology

Stamp (1940) described the seaward advance of the Irrawaddy Delta, where sandbars exist in the mouths of distributaries. The sandbars are fixed by grasses and mangroves when still under high-water levels. These sandbars become islands as a result of rapid silting, and are separated from the mainland only by narrow channels that eventually silt up. In the current distributary estuaries of the delta, the Pathein and Thetkethaung channels each have an island or a sandbar. The sandbars of the Irrawaddy, Bogale, and Toe channels are the most developed. Other distributary estuaries have few sandbars. This may mean that the Irrawaddy, Bogale, and Toe are currently the active channels in the delta.

The formation of sandbars in river mouths depends on many factors, such as fluvial conditions, tidal currents, waves, sediment grain size, and bedform characteristics (Mikhailov, 1966; Wright, 1977; Dalrymple and Choi, 2007; Leuven et al., 2018). In general, the interaction between river and tidal discharges plays a key role in the formation of sandbars in estuaries (Edmonds and Slingerland, 2007; Leonardi et al., 2013; Hoitink et al., 2017). There are two major arcuate sandbars in the Bogale estuary, and the eastern sandbar is the more prominent. Its growth and stretching orientations are consistent with those of the beach ridges of the Bogale Promontory. In addition, the eastern sandbar's evolution process is also coincident with the description of Stamp (1940). The sandbar is formed as a result of merging of several small sandbars since the 1970s. Until 2018, the southern periphery of the eastern sandbar was 14.2 km long. Its eastern end will be welded to the coast in the future. Thus, to a degree, the sandbar reflects the continuation of the delta's evolution pattern. The two sandbars have common characteristics; a sandy beach and some dunes are developed on the south side of the sandbars, and muddy intertidal deposits and tidal creeks dominate on the north side (Fig. 14g). Spits emerge, then gradually grow and bend toward land at the two ends of the sandbars. Ultimately, the sandbars become arcuate and convex seawards. The sandbars slowly move toward land and will eventually stabilize. This shape and motion may imply that at those locations, the tidal currents are dominant rather than river flow. This could be explained by the mixed wave-and-tide-dominated delta characteristics that are affected by low- to moderate-energy southwest monsoon waves (Anthony et al., 2019).

Several other sandbars and spits demonstrate the characteristics of the delta's evolution, and their evolutionary processes reflect the influences of the tide and monsoon (Fig. 14). The first is the sandbar located in the Thetkethaung estuary (Fig. 14a). Before 1974, it was a linear bar; then, the sandbar become dissected by the ebb-dominated channels. After 1990, vegetation began to grow on the sandbar. The sandbar has been cut by two barb channels in the ebb direction since 2003, and as the barb channels silted up, the sandbar developed into a tadpole shape and became stable with a long tail dragged out seaward (Fig. 14f). There were several small sandbars in the tidal channels on both sides of the tadpole-shaped sandbar. The sandbars were best developed in the tidal channel on the east side, where three U-shaped bars in the flood direction could be observed in the Landsat images of 1988 at low tidal level. Thus, the ebb-dominated channel was on the

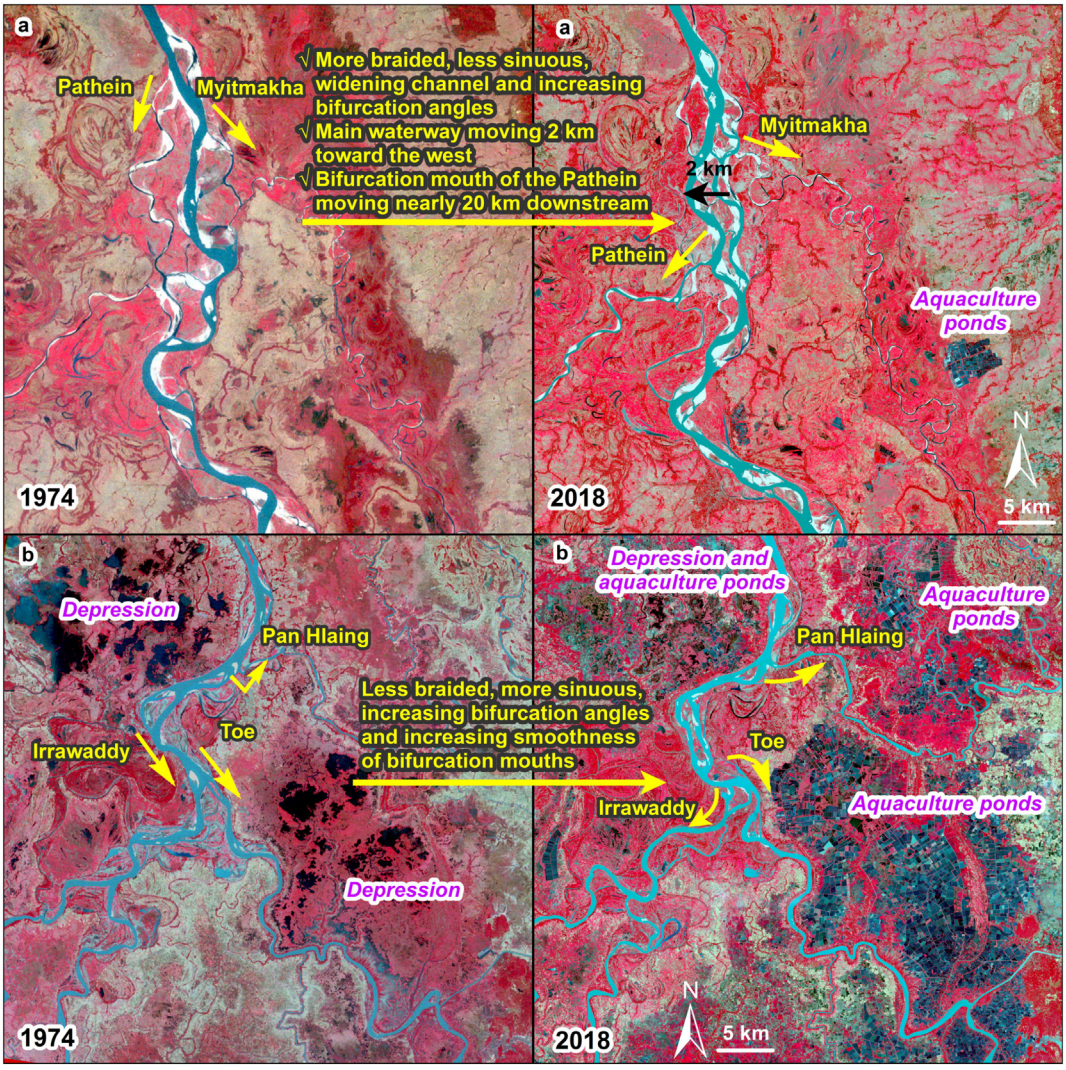

Fig. 12. Channel geomorphology at the first (a) and second (b) bifurcation points of the Irrawaddy River. The large geomorphological changes can be clearly observed from the Landsat images captured in 1974 and 2018, which display the same river reaches in subfigures (a) and (b), respectively. At the first-order bifurcation point, the changes mainly manifest as more braided, less sinuous, widening channels, increasing bifurcation angles, westward shift by approximately 2 km of the main waterway, and downstream movement of almost 20 km for the bifurcation mouth of the Pathein. At the second-order bifurcation point, the changes primarily include a less braided, more sinuous shape, increasing bifurcation angles, and smoother distributary channels. These changes in the two bifurcation points may have caused the ratio changes for water diversion into the distributaries. See Fig. 1 for locations.

west side, whereas the flood-dominated channel was on the east side. The locations, sizes, and numbers of these small sandbars in the two tidal channels varied over time. Currently, one sandbar remains visible at low tide in each channel. These features typically develop in tidal environments (Dalrymple and Rhodes, 1995; Leuven et al., 2016). The second is at the southwest coast of the Kone Gyi village tract of Labutta Township, where two recurved spits grew bilaterally from the southwest point. Here, the erosion of the coastal segment can be observed (Fig. 14b). The development of the spits was similar to that of the spits along the southwest coast of Kaingthaung Island. The third is at the southwest of the Pyin Ah Lan Village Tract of Labutta Township, where a crescent-shaped sandbar existed offshore before 1990 (Fig. 14c). Its middle section was then destroyed and merged into spits that developed afterward along the coast and were accompanied by a process of accretion. The spits then moved closer to the southwest point of the coast from both sides. The fourth exists on the east side of the Bogale Promontory, where two spits on the sides of a small stream estuary extend to the northeast (Fig. 14e). The spits stretch over 5 km toward the northeast along the coast under the influence of a littoral current. Similar geomorphological phenomena also exist further northeastward along the coast.

7. Discussion

7.1. Impacts of anthropogenic activities on sediment and hydrological regimes

7.1.1. Accelerating land use changes

Land use is a dominant driver affecting the sediment yield in a basin (Milliman and Syvitski, 1992; Russell et al., 2017). The land use in the Irrawaddy Basin has undergone tremendous changes in recent decades. Forestry and agriculture are two major land use types in the basin, providing an income source for local farmers (Htay, 2016; Veettil et al., 2018). Meanwhile, Myanmar has officially encouraged pond construction and paddy cultivation as a means of raising national incomes since the 1990s (Belton et al., 2018). Using the Hansen Global Forest Change v1.6 (2000–2018) dataset (Hansen et al., 2013) and the GEE, we found that the total forest loss was 15,338.6 km^2 from 2000 to 2018, equivalent to an annual loss of 852.1 km^2 (Fig. 15b). Seven of nine deforestation hotspots identified by Bhagwat et al. (2017) in Myanmar were located above the confluence of the Chindwin and Irrawaddy Rivers in the basin; their intact forests annually declined at a rate of 0.7% from 2002 to 2014, amounting to a total forest loss of 2589 km^2.

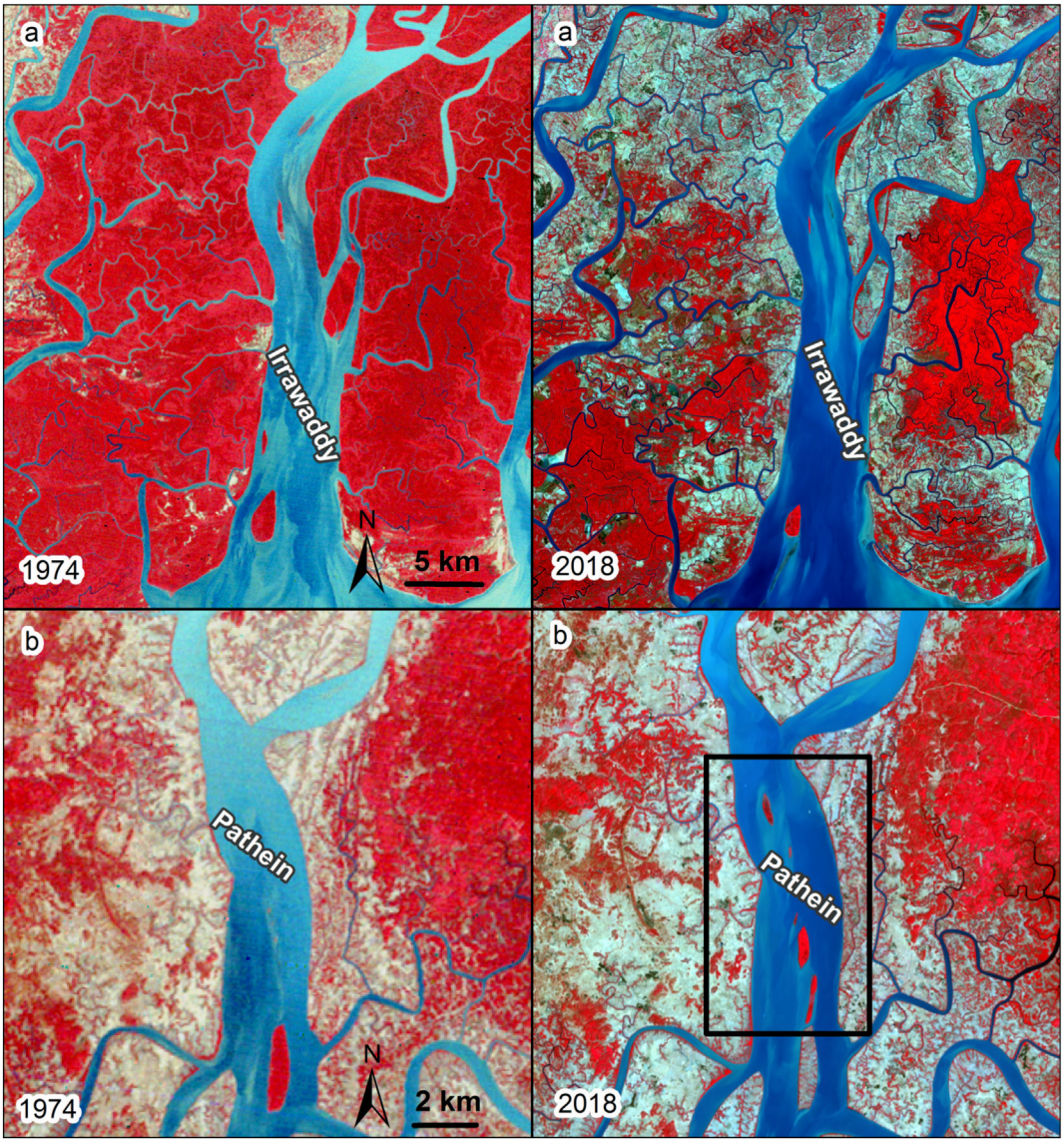

Fig. 13. (a) Eroding channel bars in the estuary reach of the Irrawaddy channel; (b) Accreting channel bars 60 km upstream of the Pathein River mouth. The underlying images are based on Landsat data captured in 1974 and 2018, which display the same river reaches in subfigures (a) and (b), respectively. The black box indicates the position of the new sandbars. See Fig. 1 for locations.

Among these casualties are mangrove forests, which had the highest deforestation rate (Wang and Myint, 2016). Mangroves are mainly located in the Lower Irrawaddy Delta, and act as natural barriers in coastal stabilization, favoring the deposition of suspended sediments and ameliorating the effects of large tropical storms and cyclones (Osti et al., 2009; Hedley et al., 2010). However, the mangrove cover in the Irrawaddy Delta has dramatically decreased by 64.2% from 1978 to 2011; 81% of originally dense mangroves were converted to rice paddies or became highly fragmented. The mangrove forests may even be completely depleted in the next 10 years (Webb et al., 2014).

This deforestation is mainly attributed to agricultural expansion and logging (Webb et al., 2014; Yang et al., 2019). Agriculture is mainly distributed in the Central Dry Zone and the Irrawaddy Delta (Torbick et al., 2017). An estimated 60% of the land area is cultivated for rice paddies in the delta region, including the Irrawaddy, Bago, and Yangon regions (Frenken, 2012). Aquaculture in the Irrawaddy Basin has also substantially increased in recent decades. According to the latest statistics from the Department of Fisheries (DOF) of Myanmar (DoF, 2018), the total area for aquaculture ponds in Myanmar was 1988.4 km^2 from 2017 to 2018. About 57% of these ponds were located in the Irrawaddy Basin, and four townships, namely Maubin, Pantanaw, and Nyaungdon Townships in Irrawaddy Division and Twantay Township in Yangon Division, occupied nearly 52% (581.6 km^2) of the basin's estimated pond area (Joffre and Kyaw, 2018) (Fig. 15a). However, the data were understated as only ponds larger than 64 m^2 were reported (Belton et al., 2018). We can clearly observe that the widespread depression in the 1970s had since been converted into intensive aquaculture ponds in 2018 in the most intensive aquaculture area near the second-order bifurcation point, with an area of 688.4 km^2 (Fig. 12).

Terrestrial mining is also a key land use activity contributing to pulses of material entering the Irrawaddy River. There are 585 mines in Myanmar, with 509 in the Irrawaddy Basin (WWF, 2018). A recent nationwide survey by EcoDev based on satellite images from 2002 to 2015 showed that there were 751.2 km^2 of potential mining areas in the Irrawaddy Basin, of which 59% were assigned a high certainty; and over 90% of the mining areas were distributed in the Chindwin, Upper, and Middle Basins, including the three divisions of Kachin, Sagaing, and Mandalay (LaJeunesse Connette et al., 2016) (Fig. 15a). The mining areas reportedly increased by 141.7% in Kachin and 743.6% in Sagaing from 2002 to 2014 (Treue et al., 2016). According to HIC (2017), the

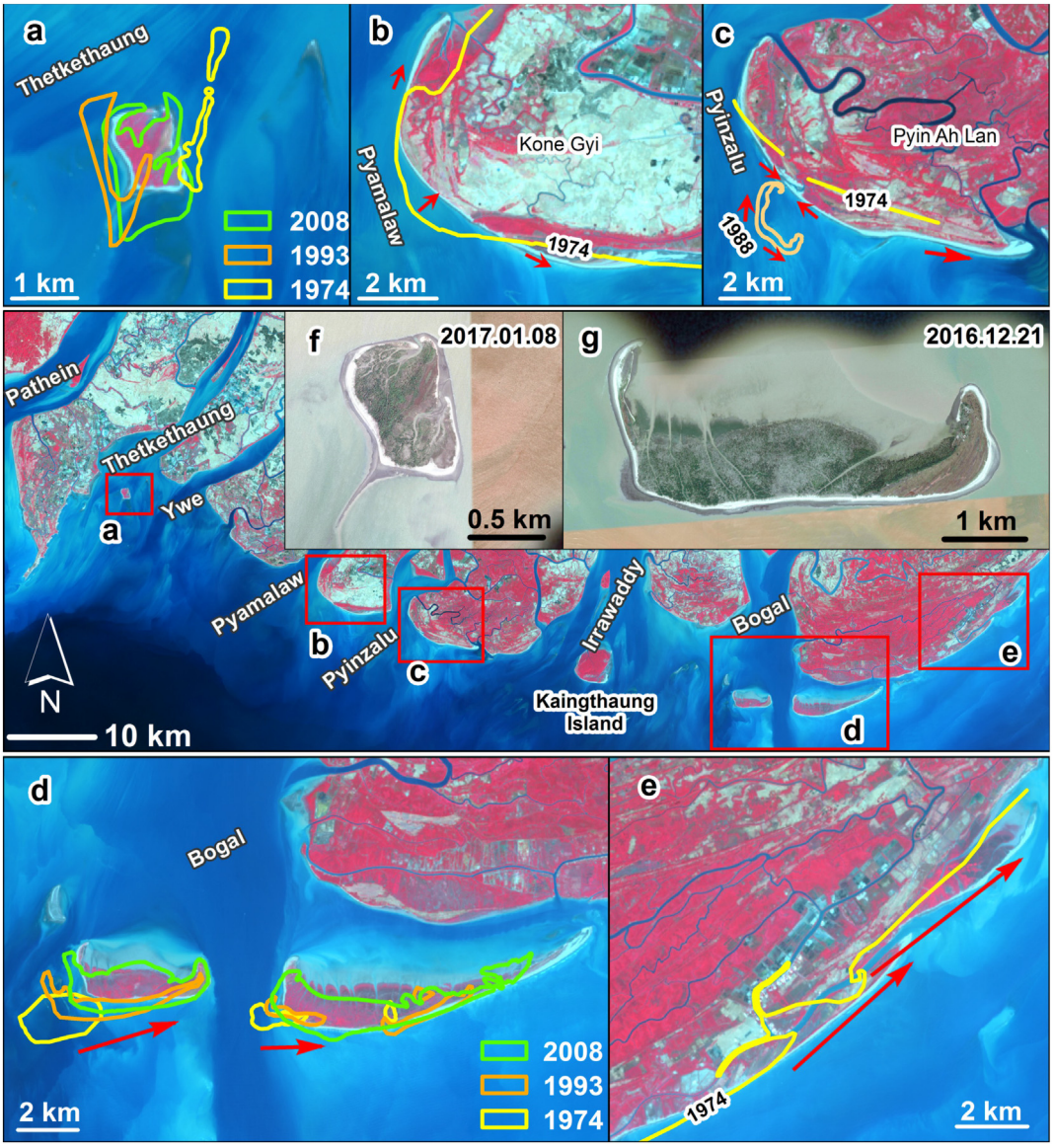

Fig. 14. Development of sandbars and spits in the estuarine area of the Irrawaddy Delta. The underlying image is based on Landsat 8 Operational Land Imager (OLI) data acquired on February 25, 2018, with a 5–4–3 band combination. (a) Tadpole-shaped sandbar forming from a submeridional elongated sandbar in the Thetkethaung estuary; (b) two recurved spits developed bilaterally from the southwest point and where the erosion of the coast segment can be observed; (c) crescent-shaped sandbar found offshore at the southwest coast of the Pyin Ah Lan Village Tract; (d) two arcuate sandbars formed in the Bogale estuary with common characteristics; (e) two spits stretching over 5 km toward the northeast along the coast under the influence of a littoral current; (f and g) close-up Google Earth images from January 8, 2017 and December 21, 2016 demonstrating the tadpole-shaped sandbar in the Thetkethaung estuary and the arcuate sandbar in the Bogale estuary. The white belts rimming the sandbars are sandy beaches and dunes.

total mining area in the Irrawaddy Basin was reached approximately 1199.3 km^2 in 2016, showing an exponential increase since 1988 (Fig. 15c). Infrastructure construction such as roads and settlements that were concomitant with mine establishment also increased. Moreover, many mining sites are now established along main waterways and tributaries, thus implying more direct impacts on the sediment supply.

The Irrawaddy has been one of the fastest eroding major basins in the world (Stamp, 1940). The deforestation, agricultural development, terrestrial mining, and associated infrastructure construction in the area may lead to more serious soil erosion. The destruction of forests will increase the occurrence of landslide events, especially in the tropical mountain regions such as the Upper Irrawaddy (Guns and Vanacker, 2013; Brakenridge et al., 2017). These potential landslide events could also contribute a significant portion, or even most, of the sediment load in some basins (Glade, 2003; Restrepo et al., 2015). Investigations found that there is a general increasing trend in the sediment grain size of bank and bed deposits downstream along the Irrawaddy River, which is unusual in river systems (HIC, 2017). The increased presence of coarse sand and gravel is probably because the area's mining activities have contributed to extra sediment input into the tributaries of the upper basin, and the episodic events during high-rainfall periods have generated substantial amounts of sediment, entering the river in the Central Dry Zone.

7.1.2. Extensive dam construction and sediment mining

Many large global river systems have experienced extensive dam construction, which is believed to be a major cause of delta erosion as a result of considerable sediment being trapped (Syvitski et al., 2009). No major dams on the trunk stream of the Irrawaddy were present during the 1990s. Since then, dam construction in the basin for hydropower and irrigation has substantially increased. In addition, to meet the needs of the growing population and correspondingly rapidly increasing economic demands in Myanmar, the construction of small and medium-

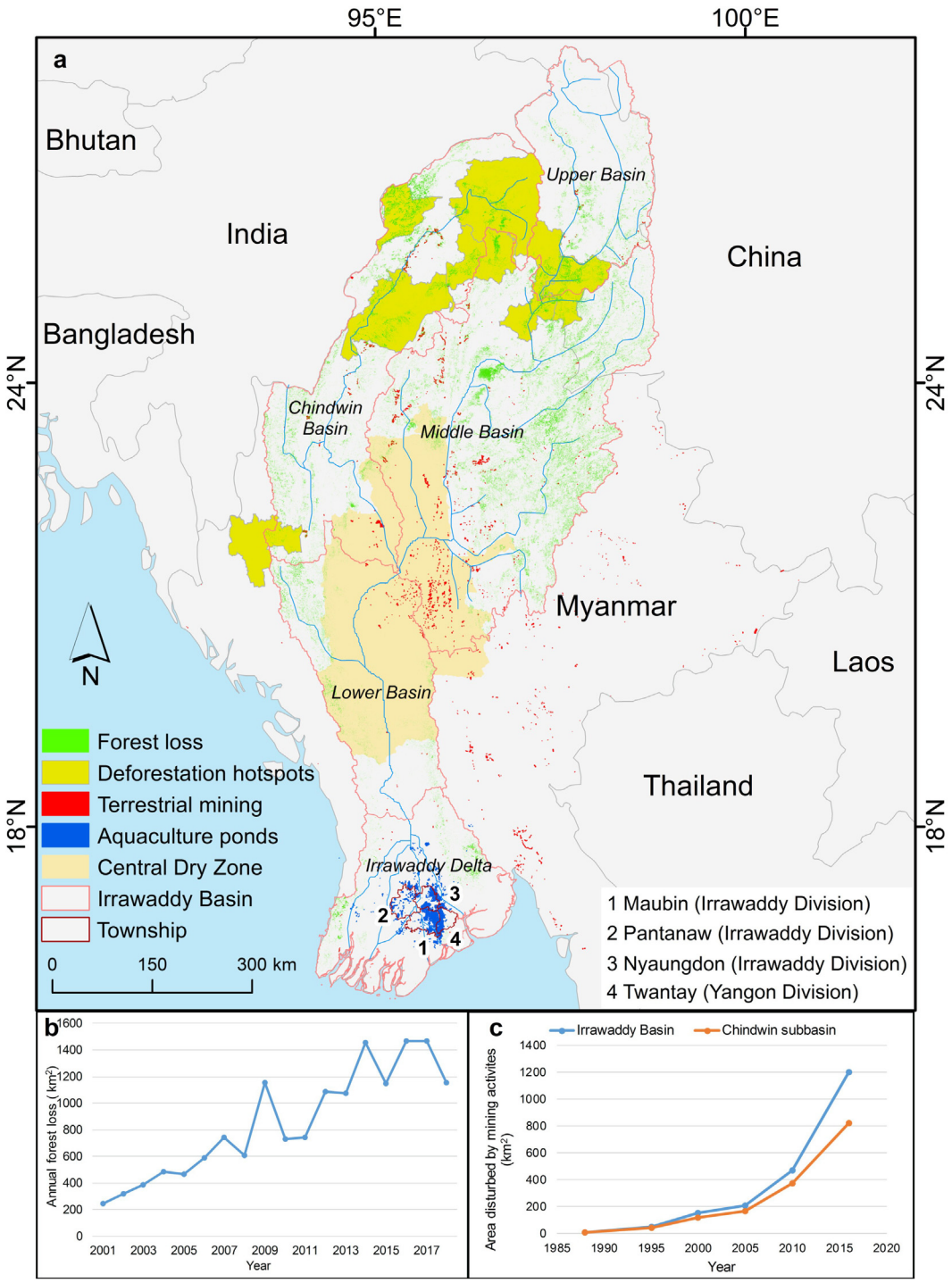

Fig. 15. (a) Significant land use changes from 1974 to 2018, including deforestation, terrestrial mining, and aquaculture. The deforestation hotspots are derived from Bhagwat et al. (2017); (b) rapid deforestation in the Irrawaddy Basin from 2000 to 2018 based on the Hansen Global Forest Change v1.6 (2000–2018) dataset (Hansen et al., 2013); (c) the land area disturbed by mining activities in the Irrawaddy Basin and Chindwin sub-basin from 1988 to 2016 (LaJeunesse Connette et al., 2016).

sized dams and irrigation projects in the tributaries of the Irrawaddy have accelerated. Currently, hydropower has become the main source of electricity in Myanmar (Nam et al., 2015). There are 35 dams in operation or under construction in Myanmar, of which 17 are in the Irrawaddy Basin, with 14 operational (2100 MW) and 3 under construction (1372 MW) (Lazarus et al., 2018) (Fig. 16). An additional 29 proposed or identified dams of 10 MW capacity or greater in the basin could potentially provide another 17,393 MW in total energy. Most are in the N'mai sub-basin, with seven dams totaling 11,395 MW, accounting for 54% of all proposed or identified dams. In addition, two proposed mainstream dams, Myitsone (6000 MW) on the Irrawaddy River and Tamanthi (1200 MW) on the Chindwin River, have been suspended by the Government of Myanmar (Lazarus et al., 2018). By the end of 2016, nearly 285 man-made reservoirs were built for hydropower and/or irrigation purposes in the Irrawaddy Basin (HIC, 2017). Incomplete statistics showed that the total storage capacity of these major reservoirs has rapidly increased from 1099×10^6 m^3 in 1985 to over $12{,}000 \times 10^6$ m^3 in 2016. If minor storages are included, the total

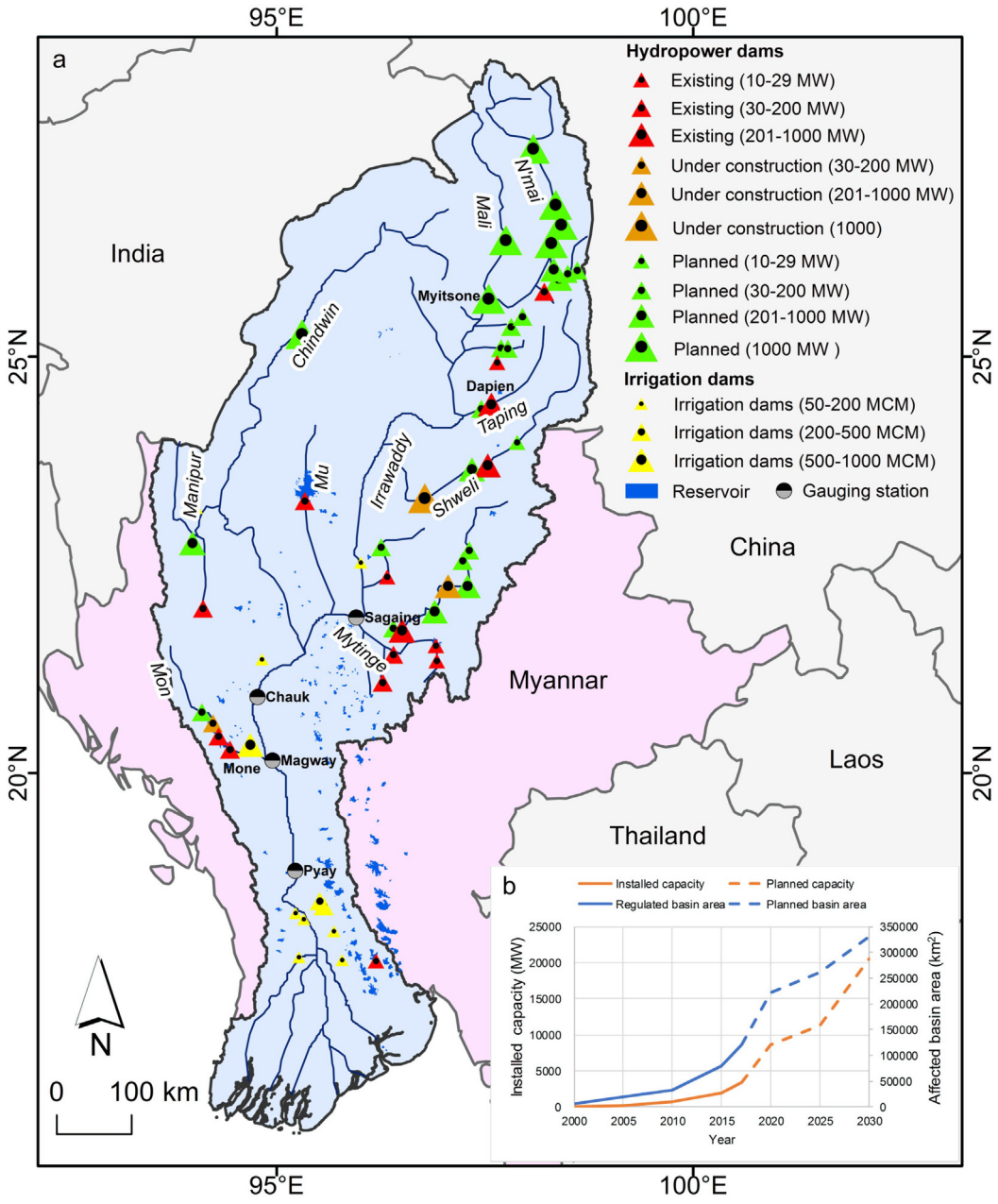

Fig. 16. (a) Distribution of dams larger than 10 MW in the Irrawaddy River Basin in 2016, adopted from HIC (2017) and Lazarus et al. (2018); (b) existing and planned hydropower projects in the Irrawaddy Basin showing the rapid increase in the installed capacity and affected basin area (HIC, 2017).

storage capacity in the basin reached 28,800 × 10^6 m^3 in 2016 (HIC, 2017). We can clearly observe from satellite images that assorted sizes of newly built reservoirs have become densely distributed across the basin in recent decades (Fig. 16).

Large-scale hydropower and irrigation projects can have substantial impacts on flow regimes and sediment loads. Although the 14 existing hydropower developments in 10 sub-basins only regulated approximately 14% of the Irrawaddy flow (Fig. 17) (Lazarus et al., 2018), the effects can be greatly increased when combined with the numerous irrigation reservoirs in the Middle and Lower Basin. At present, the inadequate observational data cannot provide definitive evidence for the impacts of dams and irrigation projects on the area's hydrology and sediment supply at the basin scale. However, local hydrological data and remote sensing observations have suggested that seasonal flows in the middle and lower reaches of the Irrawaddy River have been modified, at least at a local scale (IFC, 2017). In the future, when the planned dams are implemented, the cumulative effects will fundamentally alter the nature of the river flows and sediment transport, and eventually affect the evolution of the Irrawaddy Delta. The planned dams would result in 100% flow regulation of the Mali and N'mai headwater outflows, and still have a 43% regulation effect at the apex of the delta (Fig. 17). Notably, these upstream tributaries, which represent the major area targeted for existing and planned dams, contribute over 60% of water flow and over half of the sediment load in the basin (Stamp, 1940; HIC, 2017). A sediment supply model based on existing dams showed a significant 30% decrease in sediment load (Syvitski et al., 2009); moreover, the sediment load would experience an additional 12% decrease if all planned dams are constructed, with a potential decrease of up to 19% (Tessler et al., 2018). Therefore, dams and irrigation projects in the basin would undoubtedly modify the hydrological

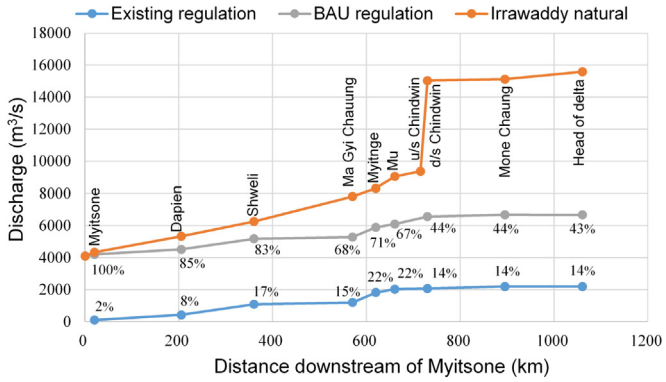

Fig. 17. Natural and regulated flows in the Irrawaddy Basin (Lazarus et al., 2018). BAU (business-as-usual) indicates "project development under the current process of project-by-project approval, with no consideration of or planning to avoid cumulative impacts on basins and sub-basins."

patterns and geomorphological and sediment transport processes along the entire downstream river course, and ultimately increase the erosion risk along the delta coast (Dunn et al., 2019).

Sediment mining along the river and beach can give rise to bank erosion, alter riverbed geomorphology, increase flooding risk, and exacerbate coastal erosion. Sediment mining is ubiquitous across the Irrawaddy Basin. Typically, coarse sand and gravel are targeted for extraction, as these are the most desirable construction materials. A gross underestimate showed that approximately 10 million tons of sediment were extracted annually from the Irrawaddy River (HIC, 2017). The actual volume was believed to be twice the this figure, namely 20 million tons or approximately 10% of the total estimated sediment load; the amount of unreported or illegal sand mining could be much larger than this budget, which could have a huge direct impact on the stability of the river bank and the delta front (WWF, 2018). A recent survey found that at least 9.4 million tons of sand and gravel were extracted in Yangon Division from 2016 to 2017 (Kadoe, 2018). A recent report confirmed that excessive sediment extraction has caused bank erosion in the Bago Region (Soe and Hammond, 2019).

7.1.3. Impacts of anthropogenic activities

With rapid growth in the population and economy, human activities have considerably affected the Irrawaddy Basin (Table 1). Satellite images show some particularly striking changes, such as the densely distributed dams for hydropower and irrigation in the peripheral regions of the basin, large-scale agricultural expansion, and mangrove deforestation in the delta region (Figs. 15 and 16). The increasing rate of dam construction and uncontrolled sediment extraction have undoubtedly reduced the sediment delivery in the river; however, large-scale deforestation and terrestrial mining have tended to increase the sediment supply, thereby offsetting the decrease in sediment load to a considerable extent (Table 1). However, because sediment data are quite scarce in the Irrawaddy Basin, it is difficult to identify the impact of a single factor on the hydrology and sediment load. Even so, local hydrological and remote sensing observations have provided evidence for hydrological and geomorphological changes at a local scale (HIC, 2017). Via detailed remote sensing observations of the entire basin, we found that the Irrawaddy River has undergone a major geomorphological adjustment through growing human activities, as inferred by Lazarus et al. (2018). As shown in Fig. 18, the main stream became less braided below the confluence with the Chindwin River in the Lower Basin, which is the high sediment yield area; the original wide, bare floodplain has been encroached by vegetation and agriculture, leaving only a narrow channel in the Central Dry Zone, and many meandering tributaries became less sinuous. And many newly dense reservoirs for irrigation or hydropower purpose are visible in the upper reaches of the tributaries. According to Mueller and Pitlick (2014), high bed-load concentrations are fundamental to maintain the braided features, which reflect a quasi-equilibrium state with a persistently high sediment supply.

Table 1
Summary of the potential influences of main human activities in the Irrawaddy Basin and its delta. In the first column, plus signs (+) indicate increasing sediment supply, whereas minus signs (−) indicate decreasing sediment supply.

Human activities	Main distribution area	Current status	Potential influences
Forest loss (+)	Chindwin, Upper, and Middle Basins	The total forest loss was 15,338.6 km^2 from 2000 to 2018.	These potential landslide events induced by deforestation could contribute a significant portion, or even most, of the sediment load in some basins (Glade, 2003; Restrepo et al., 2015).
Mangroves clearance (+)	Lower Irrawaddy Delta	The mangrove cover in the Irrawaddy Delta has dramatically decreased by 64.2% from 1978 to 2011; 81% of originally dense mangroves were converted to rice paddies or became highly fragmented. The mangrove forests may even be completely depleted in the next 10 years (Webb et al., 2014).	Mangroves clearance could lead to serious soil erosion, ultimately increase the erosion risk along the delta coast.
Agricultural development (+)	Central Dry Zone and the Irrawaddy Delta	An estimated 60% of the land area is cultivated for rice paddies in the Irrawaddy, Bago, and Yangon regions (Frenken, 2012).	The agricultural development may lead to more serious soil erosion.
Terrestrial mining (+)	Chindwin, Upper, and Middle Basins	The total mining area in the Irrawaddy Basin was reached approximately 1199.3 km^2 in 2016 (HIC, 2017).	Terrestrial mining contributes to pulses of material entering the Irrawaddy River. There is a general increasing trend in the sediment grain size of bank and bed deposits downstream along the Irrawaddy River (HIC, 2017).
dams and irrigation projects (−)	Across the basin	There are 48 dams in the Irrawaddy Basin, including 14 operational, 3 under construction, 29 proposed, and 2 suspended dams (Lazarus et al., 2018). By the end of 2016, nearly 285 man-made reservoirs were built for hydropower and/or irrigation purposes in the Irrawaddy Basin with the total storage capacity of $28{,}800 \times 10^6$ m^3 (HIC, 2017).	A sediment supply model based on existing dams showed a significant 30% decrease in sediment load (Syvitski et al., 2009); moreover, the sediment load would experience an additional 12% decrease if all planned dams are constructed, with a potential decrease of up to 19% (Tessler et al., 2018).
Sediment mining (−)	Across the basin	It was believed to be 20 million tons of sediment or approximately 10% of the total estimated sediment load were extracted annually from the Irrawaddy River (WWF, 2018). A recent survey found that at least 9.4 million tons of sand and gravel were extracted in Yangon Division from 2016 to 2017 (Kadoe, 2018).	Typically, coarse sand and gravel are targeted for sediment mining. A recent report confirmed that excessive sediment extraction has caused serious bank erosion in the Bago Region (Soe and Hammond, 2019).

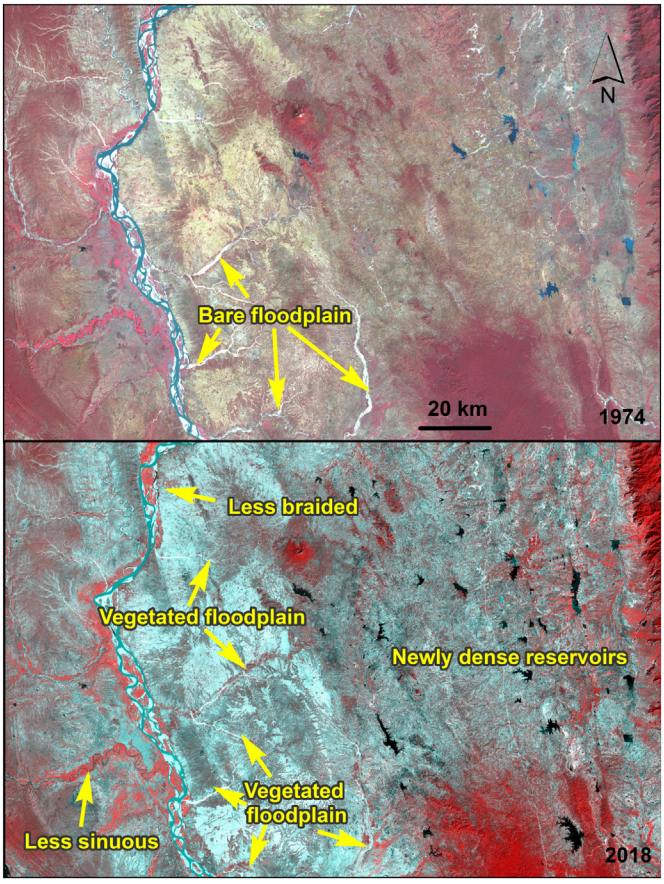

Fig. 18. Geomorphological changes of the mainstream and tributaries in the Central Dry Zone from 1974 to 2018. The less braided mainstream, less sinuous tributaries, vegetated floodplain, and newly dense reservoirs are visible. See Fig. 1 for locations.

Thus, these geomorphological adjustments are highly likely related to reductions in sediment supply (particularly coarse sand and gravel) and peak flow induced by dam construction.

Both dam construction and sediment extraction preferentially eliminate coarse sand and gravel, whereas the reduced peak flow implies that less coarse sediment is transported and enter the delta (Lazarus et al., 2018). As a result, erosion has occurred in the major channels in the lowermost delta and the western delta coast, in which sand is dominant (Anthony et al., 2019). In contrast, deforestation and terrestrial mining often provide fine sediment, which is mainly transported by the monsoon-driven current to the eastern coast, where rapidly accreting mud flats are widespread (Rao et al., 2005; Hedley et al., 2010; Giosan et al., 2018; Anthony et al., 2019). These speculations are in agreement with the findings of Hedley et al. (2010) and Giosan et al. (2018). Such transfer of fine sediment from one side to the other of the delta along its coast also occurs in many other eroding deltas, such as the Mekong (Szczuciński et al., 2013; Unverricht et al., 2013) and Indus deltas (Giosan et al., 2006).

7.2. Impacts of sediment and hydrological changes on the delta evolution

As mentioned above, geomorphological evidence and published literature demonstrated that anthropogenic activities have caused the reduction of the coarse sediment entering the Irrawaddy Delta and the extra supply of the fine sediment to the eastern coast. Such changes can potentially explain the general erosion in the western coast and the accretion in the eastern coast of the delta (Figs. 7 and 9). In addition, the sediment from the Salween (Thanlwin) and the rapid bank erosion in Sittang Rivers estuary also contributed to the accretion in the eastern coast to some extent (Shimozono et al., 2019; Liu et al., 2020). We used the incomplete sediment load data at Sagaing, Chauk, and Magway stations (IFC, 2017) (Fig. 16) to explore their relationships with the area change rates derived in Section 6.2 for Zones 1 and 2 together and Zones 1, 2, and 3 together, respectively (Fig. 19). Here, Zone 4 was not included due to the influence of other rivers. Magway station is located in the middle part of the Lower Basin, the closest to the delta coast of the three stations (Fig. 16). We calculated the correlation coefficients (r^2) between the average sediment loads during corresponding time periods and the area change rates in the two areas. The sediment load at Magway station showed the closest correlation with the area change rate. For Zones 1 and 2 together, the r^2 was 0.64, and for Zones 1, 2, and 3 together, r^2 was 0.80. Although the data are incomplete, these findings could explain the transport of fine sediment to the eastern coast to a certain extent.

For the westernmost Pathein River in Zone 1, the accreting upstream channel bars 60 km upstream of the river mouth indicated that the landward net sediment transport driven by tides in channels with little river discharge. The recent remotely monitored data from River and Reservoir Watch Version 3.5 (Brakenridge and Kettner, 2018) also showed that very little water was discharged by the Pathein River (see Section 3). In Zone 2, our results show that the channel bank and the channel bar are generally eroded (Fig. 9). The area changes of the channel bank were relatively large before 1993, since then the area changes were significantly reduced, that is, large channel adjustment occurred before 1993 (Fig. 11a). Coincidentally, the area changes of the mouth bars were relatively small before 1993, since then the mouth bars grew rapidly and obviously moved landward (Figs. 11c and 14d). These changes are likely related to reductions in sediment supply and peak flow, and relatively increase in tidal dynamics (Gugliotta and Saito, 2019). The large geomorphological adjustments at the two bifurcation points mean that the diversions and fractions of water and sediment into the distributaries have likely already changed. Fig. 12 shows that the channels became more braided and less braided at the first- and second-order bifurcation points, respectively. It implies that more coarse sediment was transmitted through the first-bifurcation point, but failed to arrive at the coastal delta plain (Leopold and Wolman, 1957; Eaton et al., 2010; Lewin and Ashworth, 2014), which can explain the erosion in the western coast to some degree. The present of coarse sediment is highly related to human activities, such as deforestation, agricultural development, terrestrial mining.

7.3. Current delta evolution pattern

This current accretion and erosion pattern of the Irrawaddy Delta is largely controlled by the regional monsoon, as stated by Rodolfo (1975). Remote sensing-derived results provide explicit evidence for this state.

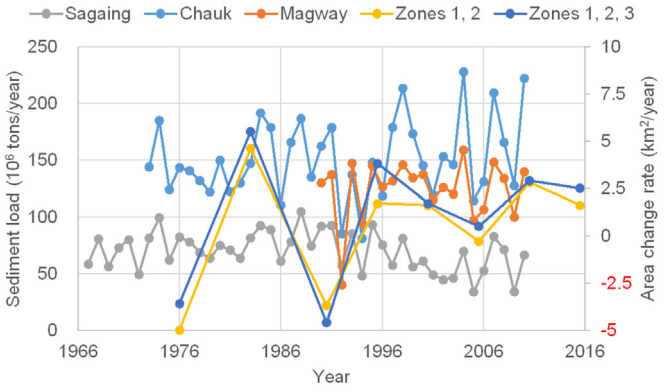

Fig. 19. Sediment loads at Sagaing, Chauk, and Magway stations (IFC, 2017) (see Fig. 16. for locations) and area change rates in Zones 1 and 2 together and Zones 1, 2, and 3 together (see Fig. 7 for locations). There are close relationships between the sediment load at Magway station and the area change rates in the two areas. For Zones 1 and 2 together, the correlation coefficient (r^2) is 0.64, and for Zones 1, 2, and 3 together, r^2 is 0.80.

The net area changes at different azimuthal angles derived from the shorelines in 1974 and 2018 and transects (Fig. 20d) show that the orientation of the erosion is mainly southwest (SW), whereas the dominant orientation of the accretion is southeast (SE). The Irrawaddy River flows from north to south, and its delta coast consists of the western coast running northwest (NW) to southeast (SE) and the embayed eastern coast running southwest (SW) to northeast (NE). The prevailing SW monsoon current drives a large amount of fine sediment into the Gulf of Martaban along the coast (Fig. 20a, b). A recent geochemical and geophysical study of sediment on the shelf also indicated that the majority of Irrawaddy River-derived sediment (83%) has been transported eastward into the Gulf of Martaban (Liu et al., 2020). Therefore, the SW of the delta coast is erodible, and the SE of the delta coast is prone to accrete.

In addition to anthropogenic impacts mentioned above, sea level rise, land subsidence, and climate change also potentially pose threats to the sustainability of the Irrawaddy Delta. There is little information about the sea level rise in the coastal sea off the delta. Mikhailov and Dotsenko (2006) reported that the water level of the Bay of Bengal rose at a rate of 1.5–2.0 mm/year. This area may experience greater sea-level rise than the global mean (Han et al., 2010). Moreover, hydrological records from the Department of Meteorology and Hydrology showed that the rising sea level has led to increased saltwater intrusions into the delta in recent years (SeinnSeinn et al., 2015). According to Horton et al. (2016), the projected sea level will reach 14–56 cm in the 2050s, which would have devastating effects on the delta shoreline. The delta has potentially been experiencing land subsidence at unknown rates (Higgins, 2016). A recent study showed that the subsidence rate was over 10 mm/year in half of Yangon City from 2014 to 2017, locally exceeding 110 mm/year (van der Horst et al., 2018). Most of the subsidence in Yangon was ascribed to groundwater extraction. The groundwater extraction in the delta region is 12% of the current recharge. Thus, expanding demand for groundwater use will potentially increase the risk of land subsidence (HIC, 2017). Recent evidence of climate change in the Irrawaddy Basin has shown its detrimental effects on the evolution of the delta. In an investigation of 130 glaciers in the Irrawaddy headwaters, Taft and Kühle (2018) found that the glaciers lost up to 54.3 ± 7.64% of their area and 60.09 ± 1.56% of their mass and volume from 1976 to 2015, and that the loss rate of the glaciers increased over time. The monsoon duration, which is one of the most influential climate factors, significantly shortened (late onset and early withdrawal) by about three weeks in northern Irrawaddy from 1988 to 2000, compared with the 1951–2000 average (McKinley et al., 2015). Other effects included rising temperatures, fewer annual rainy days, and greater frequency of intense rainfall events (McKinley et al., 2015; SeinnSeinn et al., 2015). These climate change-related events will certainly impact the hydrological regime and sediment discharge of the Irrawaddy River, and ultimately affect the stability of the delta.

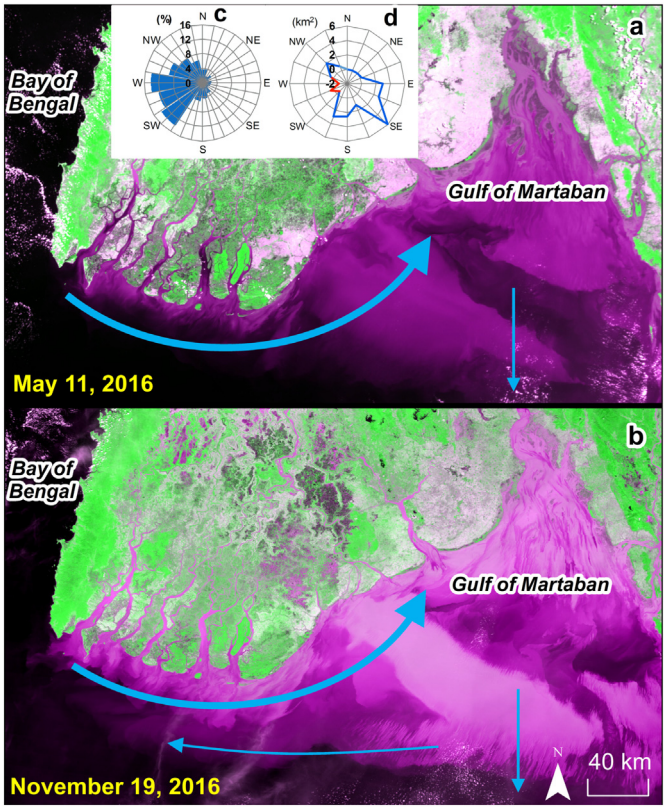

Fig. 20. Two MODIS images showing the sediment transport and dispersion patterns in the coastal sea of the Irrawaddy Delta: (a) during the SW monsoon, enormous quantities of sediment load were transported by the near-shore current eastward; (b) during the NE monsoon, the delivered sediment was mainly transported eastward into the Gulf of Martaban along the near-shore zone, whereas only a minor portion may have been pushed by surface currents westward into the Bay of Bengal; (c) wind rose diagram of the Irrawaddy delta (created based on wind data in 2016 retrieved from http://earth.nullschool.net/); (d) orientation of the accretion and erosion in the study area visually corresponding with the prevailing westerly currents generated by the SW monsoon, thereby indicating that the monsoon climate may be a major influencing factor of the delta's evolution. The blue lines indicate the direction of sediment transport adopted from Rao et al. (2005).

8. Conclusions and recommendations

With the help of Landsat images recorded over the past 44 years and the published literature, this study provides a comprehensive survey and review of the evolution of the entire Irrawaddy Delta, including its distributary channels and frontal areas. Overall, the delta's front accreted with an average shoreline change rate of 10.4 m/year from 1974 to 2018, whereas 42% of its shoreline was subject to erosion. The holistic data contain significant regional differences in the average figures. Most of the western coastline area was subjected to erosion, and only the Yangon lobe accreted prominently. However, the changes in shoreline and area did not exhibit significant trends within the delta. Notably, however, the Irrawaddy mainstream has become less braided and some tributaries have become increasingly straightened in the Lower Basin since 1974. This finding suggests that dam construction and sediment extraction most likely have caused an effective reduction of the sediment supply and alterations to the hydrological regime, although deforestation and terrestrial mining also contributed considerable amounts of fine sediment. The channel's geomorphology has undergone evident adjustments within the delta region, thereby implying that the diversions of water and sediment into the distributaries are likely to have changed. At the same time, the rising sea level has led to increasing ocean dynamics. Consequently, the delta's current equilibrium state will, in all probability, be disturbed in the near future.

We note that there is a serious dearth of scientific knowledge regarding the sediment yield and its influencing factors within the Irrawaddy Basin. The evidence from remote sensing and limited hydrological observations have indicated that human activities in the Irrawaddy Basin have exerted detrimental impacts on the sustainability of the delta. Human disturbances in the basin will continue to grow rapidly in the future as a consequence of increasing population and the pressures of economic development. This rapid growth, coupled with the potential effects of sea level rise, land subsidence, and climate change, will exacerbate erosion in the delta and increase the vulnerability of the region to extreme weather events such as floods and cyclones.

Therefore, an augmented hydrological monitoring regime that provides a baseline for future research is imperative. Survey and simulation efforts will also be conducive to unveiling the anthropogenic and natural impacts on the hydrological regime and sediment load across the basin, and remote sensing-based geomorphological surveying showed considerable advantages with its high temporal frequency, immediate

access, and wide spatial coverage. It will be very significant to quantitatively link the remote sensing-derived geomorphological changes in the delta to its fluvial and marine processes. In addition, modeling studies at the basin scale are greatly needed to address the intricate issues associated with the influences of climate change and human activities.

Declaration of competing interest

The authors declare that they have no known competing financial interests or personal relationships that could have appeared to influence the work reported in this paper.

Acknowledgments

This work was supported by the National Natural Science Foundation of China (41401093 to X. Li), US National Science Foundation under grants OCE-1737287 (J.P. Liu), the Postgraduate Research and Practice Innovation Program of Jiangsu Normal University (2018YXJ039 and KYCX18_2162), and the Priority Academic Program Development of Jiangsu Higher Education Institutions (PAPD). Special thanks go to anonymous reviewers for their valuable comments for the improvement of the manuscript.

References

Addo, K.A., Walkden, M., Mills, J.P., 2008. Detection, measurement and prediction of shoreline recession in Accra, Ghana. Isprs Journal of Photogrammetry & Remote Sensing 63 (5), 543–558.
Alongi, D.M., 2015. The impact of climate change on mangrove forests. Current Climate Change Reports 1 (1), 30–39.
Anthony, E.J., Brunier, G., Besset, M., Goichot, M., Dussouillez, P., Nguyen, V.L., 2015. Linking rapid erosion of the Mekong River delta to human activities. Sci. Rep. 5, 14745.
Anthony, E.J., Besset, M., Dussouillez, P., Goichot, M., Loisel, H., 2019. Overview of the Monsoon-influenced Ayeyarwady River delta, and delta shoreline mobility in response to changing fluvial sediment supply. Marine Geology, 106038.
Belton, B., Hein, A., Htoo, K., Kham, L.S., Phyoe, A.S., Reardon, T., 2018. The emerging quiet revolution in Myanmar's aquaculture value chain. Aquaculture 493, 384–394.
Besset, M., Anthony, E.J., Dussouillez, P., Goichot, M., 2017. The impact of Cyclone Nargis on the Ayeyarwady (Irrawaddy) River delta shoreline and nearshore zone (Myanmar): towards degraded delta resilience? Compt. Rendus Geosci. 349 (6–7), 238–247.
Bhagwat, T., Hess, A., Horning, N., Khaing, T., Thein, Z.M., Aung, K.M., Aung, K.H., Phyo, P., Tun, Y.L., Oo, A.H., 2017. Losing a jewel—rapid declines in Myanmar's intact forests from 2002–2014. PLoS One 12 (5), e0176364.
Blum, M.D., Roberts, H.H., 2009. Drowning of the Mississippi Delta due to insufficient sediment supply and global sea-level rise. Nat. Geosci. 2 (7), 488–491.
Boak, E.H., Turner, I.L., 2005. Shoreline definition and detection: a review. J. Coast. Res. 21 (4), 688–703.
Brakenridge, G.R., Kettner, A.J., 2018. River and reservoir watch version 3.4. Dartmouth Flood Observatory, University of Colorado. http://floodobservatory.colorado.edu/DischargeAccess.html.
Brakenridge, G.R., Syvitski, J.P.M., Niebuhr, E., Overeem, I., Higgins, S.A., Kettner, A.J., Prades, L., 2017. Design with nature: causation and avoidance of catastrophic flooding, Myanmar. Earth Sci. Rev. 165, 81–109.
Brichieri-Columbi, J.S.A., 1983. Hydrological studies of the Irrawaddy Delta, hydrology of humid tropical regions with particular reference to the hydrological effects of agriculture and forestry practice (Proceedings of the Hamburg Symposium, August 1983). IAHS Publ. No. 140, pp. 353–364.
Chhibber, H.L., 1934. The Geology of Burma. Macmillan, London, p. 538.
Colin, C., Bertaux, J., Turpin, L., Kissel, C., 2001. Dynamics of the erosion in the Irrawaddy River basin during the last two climatic cycles (280-0 ka). Comptes Rendus De L Academie Des Sciences Serie Ii Fascicule a-Sciences De La Terre Et Des Planetes 332 (8), 483–489.
Dalrymple, R.W., Choi, K., 2007. Morphologic and facies trends through the fluvial-marine transition in tide-dominated depositional systems: a schematic framework for environmental and sequence-stratigraphic interpretation. Earth Sci. Rev. 81 (3–4), 135–174.
Dalrymple, R.W., Rhodes, R.N., 1995. Chapter 13 estuarine dunes and bars. In: G.M.E. Perillo (Ed.), Developments in Sedimentology. Elsevier, pp. 359–422.
DoF, 2018. Fishery Statistics 2018. Department of Fisheries, Myanmar, p. 88.
Dunn, F.E., Nicholls, R.J., Darby, S.E., Cohen, S., Zarfl, C., Fekete, B.M., 2018. Projections of historical and 21st century fluvial sediment delivery to the Ganges-Brahmaputra-Meghna, Mahanadi, and Volta deltas. Sci. Total Environ. 642, 105–116.
Dunn, F.E., Darby, S.E., Nicholls, R.J., Cohen, S., Zarfl, C., Fekete, B.M., 2019. Projections of declining fluvial sediment delivery to major deltas worldwide in response to climate change and anthropogenic stress. Environ. Res. Lett. 14 (8).
Eaton, B.C., Millar, R.G., Davidson, S., 2010. Channel patterns: braided, anabranching, and single-thread. Geomorphology 120 (3), 353–364.
Edmonds, D.A., Slingerland, R.L., 2007. Mechanics of river mouth bar formation: implications for the morphodynamics of delta distributary networks. Journal of Geophysical Research: Earth Surface 112 (F2).
Fletcher, C.H., Romine, B.M., Genz, A.S., Barbee, M.M., Dyer, M., Anderson, T.R., Lim, S.C., Vitousek, S., Bochicchio, C., Richmond, B.M., 2012. National assessment of shoreline change: historical shoreline change in the Hawaiian Islands. U.S. Geological Survey Open-File Report 2011-1051, pp. 55.
Frenken, K., 2012. Irrigation in Southern and Eastern Asia in figures. AQUASTAT Survey - 2011. FAO Water Reports 37. Food and Agriculture Organization of the UN, Rome, p. 512.
Furuichi, T., Win, Z., Wasson, R.J., 2009. Discharge and suspended sediment transport in the Ayeyarwady River, Myanmar: centennial and decadal changes. Hydrol. Process. 23 (11), 1631–1641.
Garzanti, E., Wang, J.-G., Vezzoli, G., Limonta, M., 2016. Tracing provenance and sediment fluxes in the Irrawaddy River basin (Myanmar). Chem. Geol. 440, 73–90.
Giosan, L., Constantinescu, S., Clift, P.D., Tabrez, A.R., Danish, M., Inam, A., 2006. Recent morphodynamics of the Indus delta shore and shelf. Cont. Shelf Res. 26 (14), 1668–1684.
Giosan, L., Naing, T., Tun, M.M., Clift, P.D., Filip, F., Constantinescu, S., Khonde, N., Blusztajn, J.S., Buylaert, J.-P., Stevens, T., Thwin, S., 2018. On the Holocene evolution of the Ayeyawady megadelta. Earth Surface Dynamics 6, 451–466.
Glade, T., 2003. Landslide occurrence as a response to land use change: a review of evidence from New Zealand. Catena 51 (3), 297–314.
Gordon, R., 1879. Report on the Irawadi River. PW Secretar Press, Rangoon, p. 550.
Gordon, R., 1885. The Irawadi River, Proceedings of the Royal Geographical Society and Monthly Record of Geography, pp. 292–331.
Gorelick, N., Hancher, M., Dixon, M., Ilyushchenko, S., Thau, D., Moore, R., 2017. Google Earth Engine: planetary-scale geospatial analysis for everyone. Remote Sens. Environ. 202, 18–27.
Grill, G., Lehner, B., Thieme, M., Geenen, B., Tickner, D., Antonelli, F., Babu, S., Borrelli, P., Cheng, L., Crochetiere, H., Ehalt Macedo, H., Filgueiras, R., Goichot, M., Higgins, J., Hogan, Z., Lip, B., McClain, M.E., Meng, J., Mulligan, M., Nilsson, C., Olden, J.D., Opperman, J.J., Petry, P., Reidy Liermann, C., Sáenz, L., Salinas-Rodríguez, S., Schelle, P., Schmitt, R.J.P., Snider, J., Tan, F., Tockner, K., Valdujo, P.H., van Soesbergen, A., Zarfl, C., 2019. Mapping the world's free-flowing rivers. Nature 569 (7755), 215–221.
Gugliotta, M., Saito, Y., 2019. Matching trends in channel width, sinuosity, and depth along the fluvial to marine transition zone of tide-dominated river deltas: the need for a revision of depositional and hydraulic models. Earth Sci. Rev. 191, 93–113.
Guns, M., Vanacker, V., 2013. Forest cover change trajectories and their impact on landslide occurrence in the tropical Andes. Environ. Earth Sci. 70 (7), 2941–2952.
Hagenaars, G., de Vries, S., Luijendijk, A.P., de Boer, W.P., Reniers, A.J.H.M., 2018. On the accuracy of automated shoreline detection derived from satellite imagery: a case study of the sand motor mega-scale nourishment. Coast. Eng. 133, 113–125.
Halcrow, W., 1982. Irrawaddy delta hydrological investigations and delta survey - volume 3 - analysis. 94690I World Bank Group Archives, Washington, D.C., United States.
Han, W., Meehl, G.A., Rajagopalan, B., Fasullo, J.T., Hu, A., Lin, J., Large, W.G., Wang, J.-w., Quan, X.-W., Trenary, L.L., Wallcraft, A., Shinoda, T., Yeager, S., 2010. Patterns of Indian Ocean sea-level change in a warming climate. Nat. Geosci. 3, 546.
Hansen, M.C., Potapov, P.V., Moore, R., Hancher, M., Turubanova, S.A., Tyukavina, A., Thau, D., Stehman, S.V., Goetz, S.J., Loveland, T.R., Kommareddy, A., Egorov, A., Chini, L., Justice, C.O., Townshend, J.R.G., 2013. High-resolution global maps of 21st-century forest cover change. Science 342 (6160), 850–853.
Hedley, P.J., Bird, M.I., Robinson, R.A., 2010. Evolution of the Irrawaddy delta region since 1850. Geogr. J. 176 (2), 138–149.
Hennig, T., 2016. Damming the transnational Ayeyarwady basin. Hydropower and the water-energy nexus. Renewable & Sustainable Energy Reviews 65, 1232–1246.
HIC, 2017. Ayeyarwady State of the Basin Assessment (SOBA) 2017: Synthesis Report, Volume 1, Yangon, December 2017. p. 251.
Higgins, S.A., 2016. Advances in delta-subsidence research using satellite methods. Hydrogeol. J. 24 (3), 587–600.
Hoitink, A., Wang, Z., Vermeulen, B., Huismans, Y., Kästner, K., 2017. Tidal controls on river delta morphology. Nat. Geosci. 10 (9), 637.
Horton, R., De Mel, M., Peters, D., Lesk, C., Bartlett, R., Helsingen, H., Bader, D., Capizzi, P., Martin, S., Rosenzweig, C., 2016. Assessing Climate Risk in Myanmar, Center for Climate Systems Research at Columbia University. WWF-US and WWF-Myanmar, New York, NY, USA.
Htay, K.M., 2016. Mangroves in Myanmar: conflicts and impacts. In: Tantikanangkul, W., Pritchard, A. (Eds.), Politics of Autonomy and Sustainability in Myanmar: Change for New Hope…New Life?Springer Singapore, Singapore, pp. 73–90.
IFC, 2017. Baseline Assessment Report Geomorphic and Sediment Transport - Strategic Environmental Assessment of the Hydropower Sector in Myanmar. International Finance Corporation, World Bank Group.
JICA, YCDC, 2002. The Study on Improvement of Water Supply System in Yangon City in the Union of Myanmar - Final Report.
Joffre, O., Kyaw, H.A., 2018. Aquaculture in the Ayeyarwady Basin. Ayeyarwady State of the Basin Assessment (SOBA) Report 4.2. National Water Resources Committee (NWRC), Myanmar.
Kadoe, B., 2018. Exploring Sand-mining in Yangon. Status, Regulations and Impacts, Clark University, Myanmar.
Kong, D.X., Miao, C.Y., Borthwick, A.G.L., Duan, Q.Y., Liu, H., Sun, Q.H., Ye, A.Z., Di, Z.H., Gong, W., 2015. Evolution of the Yellow River Delta and its relationship with runoff and sediment load from 1983 to 2011. J. Hydrol. 520, 157–167.
Kravtsova, V.I., Mikhailov, V.N., Kidyaeva, V.M., 2009. Hydrological regime, morphological features and natural territorial complexes of the Irrawaddy River Delta (Myanmar). Water Resources 36 (3), 243–260.

Kuehl, S.A., Williams, J., Liu, J.P., Harris, C., Aung, D.W., Tarpley, D., Goodwyn, M., Aye, Y.Y., 2019. Sediment dispersal and accumulation off the Ayeyarwady delta – tectonic and oceanographic controls. Mar. Geol. 417, 106000.

Kuenzer, C., Bluemel, A., Gebhardt, S., Quoc, T.V., Dech, S., 2011. Remote sensing of mangrove ecosystems: a review. Remote Sens. 3 (5), 878.

LaJeunesse Connette, K., Connette, G., Bernd, A., Phyo, P., Aung, K.H., Tun, Y.L., Thein, Z.M., Horning, N., Leimgruber, P., Songer, M., 2016. Assessment of mining extent and expansion in Myanmar based on freely-available satellite imagery. Remote Sens. 8, 912.

Lazarus, K.M., Corbett, M., Cardinale, P., Lin, N.S., Noeske, T.K.H., 2018. Strategic Environmental Assessment of the Myanmar Hydropower Sector: Final Report. World Bank Group, Washington, D.C., p. 152.

Leonardi, N., Canestrelli, A., Sun, T., Fagherazzi, S., 2013. Effect of tides on mouth bar morphology and hydrodynamics. Journal of Geophysical Research: Oceans 118 (9), 4169–4183.

Leopold, L.B., Wolman, M.G., 1957. River Channel Patterns: Braided, Meandering, and Straight. 282B, Washington, D.C. p. 50.

Leuven, J., Kleinhans, M.G., Weisscher, S.A.H., van der Vegt, M., 2016. Tidal sand bar dimensions and shapes in estuaries. Earth Sci. Rev. 161, 204–223.

Leuven, J., De Haas, T., Braat, L., Kleinhans, M., 2018. Topographic forcing of tidal sandbar patterns for irregular estuary planforms. Earth Surf. Process. Landf. 43 (1), 172–186.

Lewin, J., Ashworth, P.J., 2014. Defining large river channel patterns: alluvial exchange and plurality. Geomorphology 215, 83–98.

Li, W., Gong, P., 2016. Continuous monitoring of coastline dynamics in western Florida with a 30-year time series of Landsat imagery. Remote Sens. Environ. 179, 196–209.

Li, X., Zhou, Y.X., Zhang, L.P., Kuang, R.Y., 2014. Shoreline change of Chongming Dongtan and response to river sediment load: a remote sensing assessment. J. Hydrol. 511, 432–442.

Li, X., Liu, J.P., Saito, Y., Nguyen, V.L., 2017. Recent evolution of the Mekong Delta and the impacts of dams. Earth Sci. Rev. 175, 1–17.

Liu, J.P., DeMaster, D.J., Nguyen, T.T., Saito, Y., Nguyen, V.P., Ta K,O,, T, Li, X., 2017. Stratigraphic formation of the Mekong River Delta and its recent shoreline changes. Oceanography 30 (3), 72–83. https://doi.org/10.5670/oceanog.2017.316.

Liu, J.P., Kuehl, S.A., Pierce, A.C., Williams, J., Blair, N.E., Harris, C., Aung, D.W., Aye, Y.Y., 2020. Fate of Ayeyarwady and Thanlwin rivers sediments in the Andaman Sea and Bay of Bengal. Mar. Geol. 423, 106137.

Login, T., 1857. 2. On the delta of the Irrawaddy. Proceedings of the Royal Society of Edinburgh, 3, 471–476.

Maiti, S., 2013. Interpretation of coastal morphodynamics of Subarnarekha estuary using integrated cartographic and field techniques. Current Science, 1709–1714.

Maiti, S., Bhattacharya, A.K., 2009. Shoreline change analysis and its application to prediction: a remote sensing and statistics based approach. Mar. Geol. 257 (1), 11–23.

McKinley, J., Adaro, C., Pede, V.O., Setiyono, T., Aung, N.M., Hom, N.H., Htwe, N.M., Hein, Y., Than, S.M., Swe, K.L., Quicho, E., Sheinkman, M., Wassmann, R., 2015. The current state of climate change perceptions and policies in Myanmar: 2014 report. CCAFS Report, CGIAR Research Program on Climate Change. Agriculture and Food Security (CCAFS), Copenhagen, Denmark.

Mikhailov, V., 1966. Hydrology and formation of river mouth bars. Problems of the Humid Tropical Zone Deltas 1, 59–64.

Mikhailov, V.N., Dotsenko, M.A., 2006. Peculiarities of the hydrological regime of the Ganges and Brahmaputra river mouth area. Water Resources 33 (4), 353–373.

Milliman, J.D., Meade, R.H., 1983. World-wide delivery of river sediment to the oceans. The Journal of Geology 91 (1), 1–21.

Milliman, J.D., Syvitski, J.P.M., 1992. Geomorphic/tectonic control of sediment discharge to the ocean: the importance of small mountainous rivers. The Journal of Geology 100 (5), 525–544.

Morton, R.A., Miller, T.L., 2005. National Assessment of Shoreline Change: Part 2, Historical Shoreline Changes and Associated Coastal Land Loss along the U.S. Southeast Atlantic Coast.

Morton, R.A., Miller, T.L., Moore, L.J., 2004. National assessment of shoreline change: Part 1: historical shoreline changes and associated coastal land loss along the US Gulf of Mexico. U.S. Geological Survey Open-file Report 2004-1043, pp. 45.

Mueller, E.R., Pitlick, J., 2014. Sediment supply and channel morphology in mountain river systems: 2. Single thread to braided transitions. Journal of Geophysical Research: Earth Surface 119 (7), 1516–1541.

Muslim, A.M., Foody, G.M., Atkinson, P.M., 2007. Shoreline mapping from coarse–spatial resolution remote sensing imagery of Seberang Takir, Malaysia. J. Coast. Res. 23 (6), 1399–1408.

Nam, K.Y., Cham, W.M., Halili, P.R., 2015. Power Sector Development in Myanmar, Asian Development Bank (ADB), Manila.

Osti, R., Tanaka, S., Tokioka, T., 2009. The importance of mangrove forest in tsunami disaster mitigation. Disasters 33 (2), 203–213.

Pardo-Pascual, J.E., Almonacid-Caballer, J., Ruiz, L.A., Palomar-Vázquez, J., 2012. Automatic extraction of shorelines from Landsat TM and ETM+ multi-temporal images with subpixel precision. Remote Sens. Environ. 123, 1–11.

Pardo-Pascual, J.E., Sánchez-García, E., Almonacid-Caballer, J., Palomar-Vázquez, J.M., Priego de los Santos, E., Fernández-Sarría, A., Balaguer-Beser, Á., 2018. Assessing the accuracy of automatically extracted shorelines on microtidal beaches from Landsat 7, Landsat 8 and Sentinel-2 imagery. Remote Sens. 10 (2), 326.

Phan, L.K., van Thiel de Vries, J.S.M., Stive, M.J.F., 2015. Coastal mangrove squeeze in the Mekong Delta. J. Coast. Res. 31 (2), 233–243.

Ramaswamy, V., Rao, P.S., Rao, K.H., Thwin, S., Rao, N.S., Raiker, V., 2004. Tidal influence on suspended sediment distribution and dispersal in the northern Andaman Sea and Gulf of Martaban. Mar. Geol. 208 (1), 33–42.

Rao, P.S., Ramaswamy, V., Thwin, S., 2005. Sediment texture, distribution and transport on the Ayeyarwady continental shelf, Andaman Sea. Mar. Geol. 216 (4), 239–247.

Restrepo, J.D., Kettner, A., Syvitski, J.P., 2015. Recent deforestation causes rapid increase in river sediment load in the Colombian Andes. Anthropocene 10, 13–28.

Robinson, R.A.J., Bird, M.I., Oo, N.W., Hoey, T.B., Aye, M.M., Higgitt, D.L., Lu, X.X., Swe, A., Tun, T., Win, S.L., 2007. The Irrawaddy River sediment flux to the Indian Ocean: the original nineteenth-century data revisited. J. Geol. 115 (6), 629–640.

Rodolfo, K.S., 1975. The Irrawaddy Delta: Tertiary Setting and Modern Offshore Sedimentation, Deltas: Models for Exploration. pp. 329–348.

Romine, B.M., Fletcher, C.H., Frazer, L.N., Genz, A.S., Barbee, M.M., Lim, S.C., 2009. Historical shoreline change, Southeast Oahu, Hawaii; applying polynomial models to calculate shoreline change rates. J. Coast. Res. 25 (6), 1236–1253.

Russell, K.L., Vietz, G.J., Fletcher, T.D., 2017. Global sediment yields from urban and urbanizing watersheds. Earth Sci. Rev. 168, 73–80.

SeinnSeinn, M., Ahmad, M., Thapa, G., Shrestha, R., 2015. Farmers' adaptation to rainfall variability and salinity through agronomic practices in lower Ayeyarwady Delta, Myanmar. Journal of Earth Science & Climatic Change 6 (2), 258.

Shearman, P., Bryan, J., Walsh, J.P., 2013. Trends in deltaic change over three decades in the Asia-Pacific region. J. Coast. Res. 29 (5), 1169–1183.

Shimozono, T., Tajima, Y., Akamatsu, S., Matsuba, Y., Kawasaki, A., 2019. Large-scale channel migration in the Sittang River estuary. Sci. Rep. 9 (1), 9862.

Soe, H.K., Hammond, C., 2019. Myanmar's Ayeyarwady River at Risk From Rampant Sand Mining (Earth Journalism Network, 2019).

Souza, P.W.M., Martins, E.D., da Costa, F.R., 2006. Using mangroves as a geological indicator of coastal changes in the Braganca macrotidal flat, Brazilian Amazon: a remote sensing data approach. Ocean & Coastal Management 49 (7–8), 462–475.

Stamp, L.D., 1925. The aerial survey of the Irrawaddy Delta Forests (Burma): notes embracing the observations of Messrs. A. W. Moodie C. R. Robbins and C. W. Scott, compiled and edited with permission. J. Ecol. 13 (2), 262–276.

Stamp, L.D., 1940. The Irrawaddy River. Geogr. J. 95 (5), 329–352.

Stanley, D.J., Warne, A.G., 1993. Nile delta: recent geological evolution and human impact. Science 260 (5108), 628–634.

Syvitski, J.P.M., Kettner, A.J., Overeem, I., Hutton, E.W.H., Hannon, M.T., Brakenridge, G.R., Day, J., Vörösmarty, C., Saito, Y., Giosan, L., Nicholls, R.J., 2009. Sinking deltas due to human activities. Nat. Geosci. 2 (10), 681–686.

Syvitski, J.P.M., Overeem, I., Brakenridge, G.R., Hannon, M., 2012. Floods, floodplains, delta plains — a satellite imaging approach. Sediment. Geol. 267–268, 1–14.

Syvitski, J.P.M., Cohen, S., Kettner, A.J., Brakenridge, G.R., 2014. How important and different are tropical rivers? — an overview. Geomorphology 227, 5–17.

Szczuciński, W., Jagodzinski, R., Hanebuth, T.J.J., Stattegger, K., Wetzel, A., Mitrega, M., Unverricht, D., Phung, P.V., 2013. Modern sedimentation and sediment dispersal pattern on the continental shelf off the Mekong River delta, South China Sea. Glob. Planet. Chang. 110, 195–213.

Taft, L., Kühle, L., 2018. Glacier changes between 1976 and 2015 in the source area of the Ayeyarwady (Irrawaddy) River, Myanmar. Water 10 (12), 1850.

Tamura, T., Saito, Y., Bateman, M.D., Nguyen, V.L., Ta, T.K.O., Matsumoto, D., 2012. Luminescence dating of beach ridges for characterizing multi-decadal to centennial deltaic shoreline changes during Late Holocene, Mekong River delta. Mar. Geol. 326, 140–153.

Tanabe, S., Saito, Y., Sato, Y., Suzuki, Y., Sinsakul, S., Tiyapairach, S., Chaimanee, N., 2003. Stratigraphy and Holocene evolution of the mud-dominated Chao Phraya delta, Thailand. Quat. Sci. Rev. 22 (8–9), 789–807.

Tanabe, S., Saito, Y., Vu, Q.L., Hanebuth, T.J.J., Ngo, Q.L., Kitamura, A., 2006. Holocene evolution of the Song Hong (Red River) delta system, northern Vietnam. Sediment. Geol. 187 (1–2), 29–61.

Tessler, Z.D., Vorosmarty, C.J., Overeem, I., Syvitski, J.P.M., 2018. A model of water and sediment balance as determinants of relative sea level rise in contemporary and future deltas. Geomorphology 305, 209–220.

Thieler, E.R., Himmelstoss, E.A., Zichichi, J.L., Ergul, A., 2017. Digital Shoreline Analysis System (DSAS) version 4.0—An ArcGIS extension for calculating shoreline change (ver. 4.4, July 2017). U.S. Geological Survey Open-File Report 2008-1278.

Torbick, N., Chowdhury, D., Salas, W., Qi, J., 2017. Monitoring rice agriculture across Myanmar using time series Sentinel-1 assisted by Landsat-8 and PALSAR-2. Remote Sens. 9 (2), 119.

Treue, T., Springate-Baginski, O., Htun, K., 2016. Legally and Illegally Logged Out: Extent and Drivers of Deforestation and Forest Degradation in Myanmar.

Unverricht, D., Szczuciński, W., Stattegger, K., Jagodzinski, R., Le, X.T., Kwong, L.L.W., 2013. Modern sedimentation and morphology of the subaqueous Mekong Delta, Southern Vietnam. Glob. Planet. Chang. 110, 223–235.

van der Horst, T., Rutten, M.M., van de Giesen, N.C., Hanssen, R.F., 2018. Monitoring land subsidence in Yangon, Myanmar using Sentinel-1 persistent scatterer interferometry and assessment of driving mechanisms. Remote Sens. Environ. 217, 101–110.

Veettil, B.K., Ruiz Pereira, S.F., Quang, N.X., 2018. Rapidly diminishing mangrove forests in Myanmar (Burma): a review. Hydrobiologia 822 (1), 19–35.

Vörösmarty, C.J., Syvitski, J., Day, J., De Sherbinin, A., Giosan, L., Paola, C., 2009. Battling to save the world's river deltas. Bull. At. Sci. 65 (2), 31–43.

Wang, C.Y., Myint, S.W., 2016. Environmental concerns of deforestation in Myanmar 2001–2010. Remote Sens. 8 (9), 728.

Webb, E.L., Jachowski, N.R.A., Phelps, J., Friess, D.A., Than, M.M., Ziegler, A.D., 2014. Deforestation in the Ayeyarwady Delta and the conservation implications of an internationally-engaged Myanmar. Glob. Environ. Chang. 24, 321–333.

Webster, P.J., 2008. Myanmar's deadly daffodil. Nat. Geosci. 1, 488–490.

Wright, L., 1977. Sediment transport and deposition at river mouths: a synthesis. Geol. Soc. Am. Bull. 88 (6), 857–868.

WWF, 2018. The Ayeyarwady River and the economy of Myanmar, vol. 1: Risks and Opportunities From the Perspective of People Living and Working in the Basin, pp. 21.

Yang, S.L., Milliman, J.D., Li, P., Xu, K., 2011. 50,000 dams later: erosion of the Yangtze River and its delta. Glob. Planet. Chang. 75 (1–2), 14–20.

Yang, R., Luo, Y., Yang, K., Hong, L., Zhou, X., 2019. Analysis of forest deforestation and its driving factors in Myanmar from 1988 to 2017. Sustainability 11 (11), 3047.